JOURNAL OF PETROLOGY | VOLUME 52 | NUMBER 2 | PAGES 223–256 | 2011 | doi:10.1093/petrology/egq078

Assessing Bulk Assimilation in Cordierite-bearing Granitoids from the Central System Batholith, Spain; Experimental, Geochemical and Geochronological Constraints

JUAN DÍAZ-ALVARADO[1], ANTONIO CASTRO[2]*, CARLOS FERNÁNDEZ[1] AND IGNACIO MORENO-VENTAS[2]

[1]DEPARTAMENTO DE GEODINÁMICA Y PALEONTOLOGÍA, UNIVERSIDAD DE HUELVA, CAMPUS DEL CARMEN, 21071 HUELVA, SPAIN

[2]DEPARTAMENTO DE GEOLOGÍA, UNIVERSIDAD DE HUELVA, CAMPUS DEL CARMEN, 21071 HUELVA, SPAIN

RECEIVED APRIL 13, 2010; ACCEPTED NOVEMBER 4, 2010
ADVANCE ACCESS PUBLICATION DECEMBER 14, 2010

This paper describes in detail an example of a calc-alkaline batholith, located in the Gredos massif (Spanish Central system batholith, Iberian Variscan massif), intruded into pelitic metasediments at shallow crustal levels. The igneous rocks of the study area are divided into three main groups according to their petrographic and geochemical (major, trace and rare earth element) characteristics: calc-alkalic (Qtz diorites and tonalites), transitional (Bt granodiorites), and alkali-calcic series (typically composed of Crd monzogranites). A paradoxical feature of the Crd monzogranites is the presence of euhedral Crd crystals in strong disequilibrium within a non-anatectic monzogranite. The field relations and geochemical data strongly suggest a process of bulk assimilation of the host metasediments by the intruding Bt granodiorites to generate the Crd monzogranites. Geochemical trends defined by the Crd monzogranites clearly depart from cotectic-like evolutions of liquid composition, and point to the composition of the metapelitic host-rocks. Laboratory experiments have been performed to check this hypothesis, and the results show that cordierite forms in a local domain where the reactants of the peritectic reaction $Bt + Qtz + Pl + Als \rightarrow Crd + Kfs + Melt$ *are located. The process includes the isolation of metapelitic xenoliths in the granodiorite magma (a feature observed in the field), partial melting of these xenoliths with generation of cordierite as a peritectic phase in local equilibrium with the melt inside the entrapped xenolith, and the survival of these crystals because the residual melt of the granodiorite magma converges compositionally toward the peraluminous leucogranite generated in the relic xenolith. In turn, the granodiorite gains K released from the xenoliths, inducing the crystallization of K-feldspar and shifting to a Crd monzogranitic composition. Inherited zircons are present in the Crd monzogranites, similar to those found in the host metasediments; these are virtually absent in the intrusive Bt granodiorites. Mass-balance calculations and estimates based on the amount of Crd present have been applied to quantify the extent of assimilation in the petrogenesis of the granitoids; the volume of assimilated material can be high, depending on the proximity to the contacts with the xenoliths and the amount of pelitic material in the metasediments.*

KEY WORDS: *assimilation; granodiorite; experimental petrology; geochemistry; cordierite; geochronology*

INTRODUCTION

Reactive bulk assimilation has been proposed as an efficient mechanism to account for large chemical and mineralogical modifications in granitoids without large energy requirements (Beard *et al.*, 2005; Erdmann *et al.*, 2007; Saito *et al.*, 2007). The basic principle is that fragments of the surrounding country rocks (xenoliths), trapped by the intruding magma, may disaggregate if a

*Corresponding author. E-mail: dorado@uhu.es

moderate melt fraction (*c.* 20–30 vol. %) is formed within them, allowing residual crystals to disperse mechanically within the magma. In the common case of deep-crust generated granite magma intruding into upper crust dominantly composed of pelitic metasediments, there is an important mineralogical similarity between the residual phases in the assimilated xenoliths, specifically Qtz, Pl, Bt, Kfs, Crd ± Grt [mineral abbreviations after Kretz (1983)] and the phases crystallizing in the intruding magma (Pl, Qtz, Bt, Kfs). Additionally, the melt produced in the trapped xenoliths can be close in composition (peraluminous leucogranite) to the residual melt of the intruding magma, even if this melt is not affected by pelite assimilation; in both cases the melt composition is dictated by the thermodynamic minimum in the system Qtz–Ab–Or–H_2O (Tuttle & Bowen, 1958; Johannes & Holtz, 1996; Winkler & Lindemann, 1972). With the exception of the peritectic phase Crd (or Grt at *P* higher than 400–600 MPa) formed by incongruent melting of Bt in presence of Als (Le Breton & Thompson, 1988; Vielzeuf & Holloway, 1988) the other mineral phases are not easily recognizable in the resulting contaminated granitoid. Consequently, the presence of Crd, together with other complementary geological and petrological observations, can be considered as a diagnostic feature of assimilation and, for this reason, the formation of Crd has received considerable attention in the study of granitoids (Ugidos & Recio, 1993; Clarke, 1995; Erdmann *et al.*, 2007; Ugidos *et al.*, 2008). This attention is particularly relevant where Crd occurs in granitoids that have compositions that depart considerably (e.g. tonalites: Saito *et al.*, 2007; monzogranites and granodiorites: García-Moreno *et al.*, 2006; Ugidos *et al.*, 2008) from the typical peraluminous leucogranite composition of melts formed by peritectic reactions (Bt breakdown) in pelitic migmatites in both nature (Patiño Douce, 1992; Pereira & Bea, 1994) and experiments (Vielzeuf & Holloway, 1988; Patiño-Douce & Johnston, 1991; Patiño Douce, 1999; Castro *et al.*, 2000).

The aim of this study is to assess the extent of assimilation in a batholith context. We describe here a magnificent example of a calc-alkaline batholith, generated from a deep crustal source region, which intruded pelitic rocks at a shallow crustal level during the late (transcurrent and extensional) stages of the Variscan orogeny in Central Spain.

The tectono-metamorphic evolution in the Central System batholith includes three main ductile deformation phases: D_1 (upright folds, contractional deformation) (Dallmeyer *et al.*, 1997; Escuder Viruete *et al.*, 1998), 360?–337 Ma; D_2 (extensional detachments) (Escuder Viruete *et al.*, 1994, 1998; Dallmeyer *et al.*, 1997; Martínez Catalán *et al.*, 2004; Castiñeiras *et al.*, 2008), 337–320 Ma; D_3 (upright folds and transcurrent shear zones) (Días *et al.*, 1998), 320–300 Ma. The metamorphic peak and migmatization took place coeval with or slightly later than the D_2 phase (Escuder Viruete *et al.*, 1998; Montero *et al.*, 2004; Bea *et al.*, 2006; Castiñeiras *et al.*, 2008).

A combined study including field relations, geochemistry, experimental simulations and phase equilibria, and sensitive high-resolution ion microprobe (SHRIMP) zircon studies has been conducted in the Gredos massif (Central Spain), one of the best outcrops of the Central System batholith. Important paradoxes concerning the texture and composition of Crd-bearing granitoids can be resolved based on the results of this study. Cordierite is a characteristic mineral in low-pressure migmatites and peraluminous granites. It is a diagnostic phase of S-type granites formed during anatexis of pelitic metasediments (Chappell & White, 1974) by incongruent melting reactions. The generation of cordierite at supersolidus conditions is controlled by the bivariant prograde peritectic reaction

$$\mathrm{Bt} + \mathrm{Qtz} + \mathrm{Pl} + \mathrm{Als} \rightarrow \mathrm{Crd} + \mathrm{Kfs} + \mathrm{Melt}. \qquad (1)$$

This reaction has been extensively studied experimentally (Thompson, 1982, 1996; Vielzeuf & Holloway, 1988; Patiño Douce & Johnston, 1991; Castro *et al.*, 2000) and evidenced by textural and mineralogical studies in pelitic migmatites and their associated peraluminous granites (Clarke, 1995; Barbey *et al.*, 1999). However, some granodiorite and monzogranite rocks with calc-alkaline affinity, including Hbl-bearing Qtz diorites, diorites, gabbros and mafic microgranular enclaves (I-type granites, Chappell & White, 1974), may locally contain large euhedral (magmatic?) crystals of Crd. The paradoxical occurrence of this typically anatectic mineral in these granites, apparently unrelated genetically to the anatectic domain in which they are emplaced, in apparently textural equilibrium as denoted by their euhedral prismatic shape and homogeneous grain size, but far from chemical equilibrium with the host magma (García-Moreno *et al.*, 2006), has been the object of intense debate. A xenocrystic or peritectic xenocrystic origin has been proposed for Crd in such plutonic rocks of granodiorite to monzogranite composition (Ugidos & Recio, 1993). We present here the results of new laboratory experiments simulating the process of assimilation and simultaneous crystallization of Crd in granitoids from the Gredos massif. These experiments are similar to those previously reported (Erdmann *et al.*, 2007) at lower pressures (200 MPa) and under water-saturation conditions. Distinct situations of bulk and selective assimilation processes are tested with experimental simulations. The new experiments described here were conducted at pressures of 400 MPa under water-undersaturated conditions that are assumed to prevail at the level of emplacement in the upper crust where interaction with metasediments took place.

PREVIOUS WORK: GEOLOGICAL SETTING, MAIN UNITS AND FIELD RELATIONS

The Gredos massif is part of a huge granite–granodiorite batholith, more than 300 km long and 60 km wide, that crops out in central Spain, from the Madrid region to South Salamanca province and North Extremadura (Fig. 1a). Continuous granitic exposures form a great part of the Alpine mountains of the Spanish Central System, and so the batholith is normally referred to as the Central System batholith (Castro *et al.*, 2002). As in many other batholiths of similar composition (e.g. Newer Caledonian granites in Scotland: Stephens & Halliday, 1984; French Massif Central: Didier & Lameyre, 1969; Pin & Duthou, 1990; Western Australia: Collins, 1996), these calc-alkaline batholiths are always late orogenic, postdating by more than 20 Myr the major orogenic phases.

One of the most distinctive features of the Central System batholith is the presence of low-*P* metamorphic complexes that form large (>20 km long) roof-pendants in the centre and margins of the batholith (Fig. 1a). Here low-grade metasediments are metamorphosed into migmatitic hornfelses locally surrounding the granitoid intrusions. Elsewhere high-grade complexes are characterized by the association of upper crustal migmatites with anatectic granites (S-type). Most of these migmatites are derived from pelitic and semipelitic metasediments that form part of the several kilometres thick Neo-Proterozoic turbiditic series and Ordovician ferrosilicic metavolcanic series (Fernández *et al.*, 2008) that are widely represented in the Iberian massif in Spain and Portugal. In some places, as in the case of this study area, both migmatitic hornfelses and regional, high-grade migmatites occur close together. This suggests that granitoid intrusion took place in a previously structured domain in which large extensional detachment faults brought low-grade metasediments and anatectic complexes into contact. Interaction between intruding sheets of granodiorite and the surrounding metasediments is common, making this area one of special interest for the study of crustal assimilation processes (Ugidos & Recio, 1993; Ugidos *et al.*, 2008). Although local, the complex geometry of the contacts and the multiple pulses of magma intrusion in kilometre-sized layered structures make the 'local' interaction a common process in this batholith.

Large homogeneous volumes of coarse-grained, porphyritic granitic rocks of granodiorite to monzogranite composition constitute more than 90 vol. % of the intrusive rocks. Minor amounts of more basic rocks ranging from gabbro to Qtz diorite are present elsewhere in the batholith, some of them being locally dominant over kilometre-sized irregular areas, but dominantly concentrated close to the contacts with the country rocks. In general, all the plutonic rocks from gabbros to granodiorites form a typical K-rich calc-alkaline association (Moreno-Ventas *et al.*, 1995) having close similarities to typical Caledonian I-type batholiths (Chappell & Stephens, 1988), and belonging to the large group of Variscan intrusive rocks catalogued as 'calc-alkaline series granitoids' in regional syntheses and classifications of the Variscan magmatism (Capdevila *et al.*, 1973; Castro *et al.*, 2002). According to the Frost *et al.* (2001) classification scheme, the intrusive units are of magnesian-type and evolve from typical calc-alkalic (CA) to alkali-calcic (AC) series (Fig. 2b). Hornblende-bearing rocks, Bt tonalites and some of the Bt granodiorites are calc-alkalic and the Hbl-diorites are metaluminous [alumina saturation index (ASI) < 1]. These are referred to as the calc-alkalic intrusive unit (CAIU) subsequently. Most of the Bt granodiorites and monzogranites are transitional between calc-alkalic and alkali-calcic series (Frost *et al.*, 2001) and have moderate peraluminosity (1 <ASI <1·2) (Fig. 2a). These rocks are grouped together in a single unit called the transitional intrusive unit (TIU). The Crd-bearing unit is characteristically composed of monzogranites (Fig. 2c). They are more peraluminous (ASI >1·2) and plot in the alkali-calcic field (Fig. 2b). They will be referred to as the alkali-calcic unit (ACU). Other magmatic rocks, not included in this study, include mafic microgranular enclaves that are widespread in all rock types of the CAIU and TIU. They are also present, but less abundant, in the Crd monzogranites of the ACU. Many of these enclaves are true autoliths that represent fragments of early magmatic pulses that were quenched against the country rocks and were subsequently dismembered by successive magma pulses by magmatic erosion (Paterson & Janousek, 2008).

Field relations of the granitoids and country rocks

Figure 1b shows a detailed geological map of the central part of the batholith (Sierra de Gredos, location shown in Fig. 1a). Far from being massive and homogeneous, the granitoids of the TIU and ACU in this region are well structured in parallel layers of variable thickness, commonly approaching 1 km. Alternating layers of migmatite and granitoid are affected by at least two generations of folds, which cause a complex fold interference pattern (Fig. 1b and c). Rare structures indicative of solid-state deformation can be seen in the granitoid layers, although ductile shear zones have been occasionally observed in some contacts between granitoids and migmatites.

Two main granitoid layers (called here Las Pozas and Barbellido; Fig. 1b) have been identified in the mapped area. The Las Pozas Crd monzogranite is a tabular body, around 800 m thick, sandwiched between two migmatite layers. Several septa of migmatitic hornfels are included within the Las Pozas Crd monzogranite, particularly near

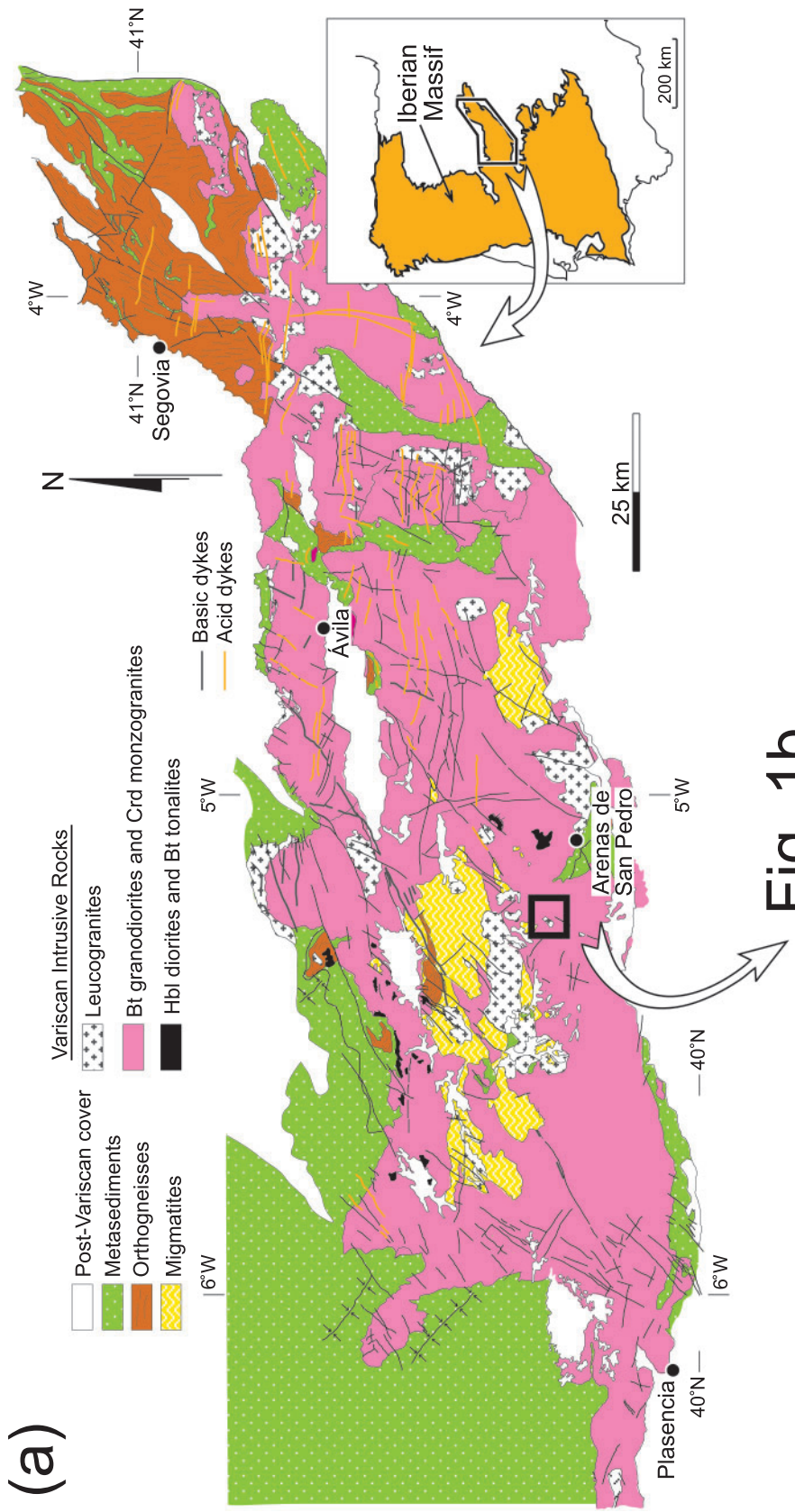

Fig. 1. (a) Geological map of the Spanish Central System batholith. (b) Detailed geological map of the Barbellido–Las Pozas area (Sierra de Gredos, Central System batholith). Location indicated by rectangle in (a). (c) WNW–ESE-trending geological cross-section showing the main structural features of the mapped area.

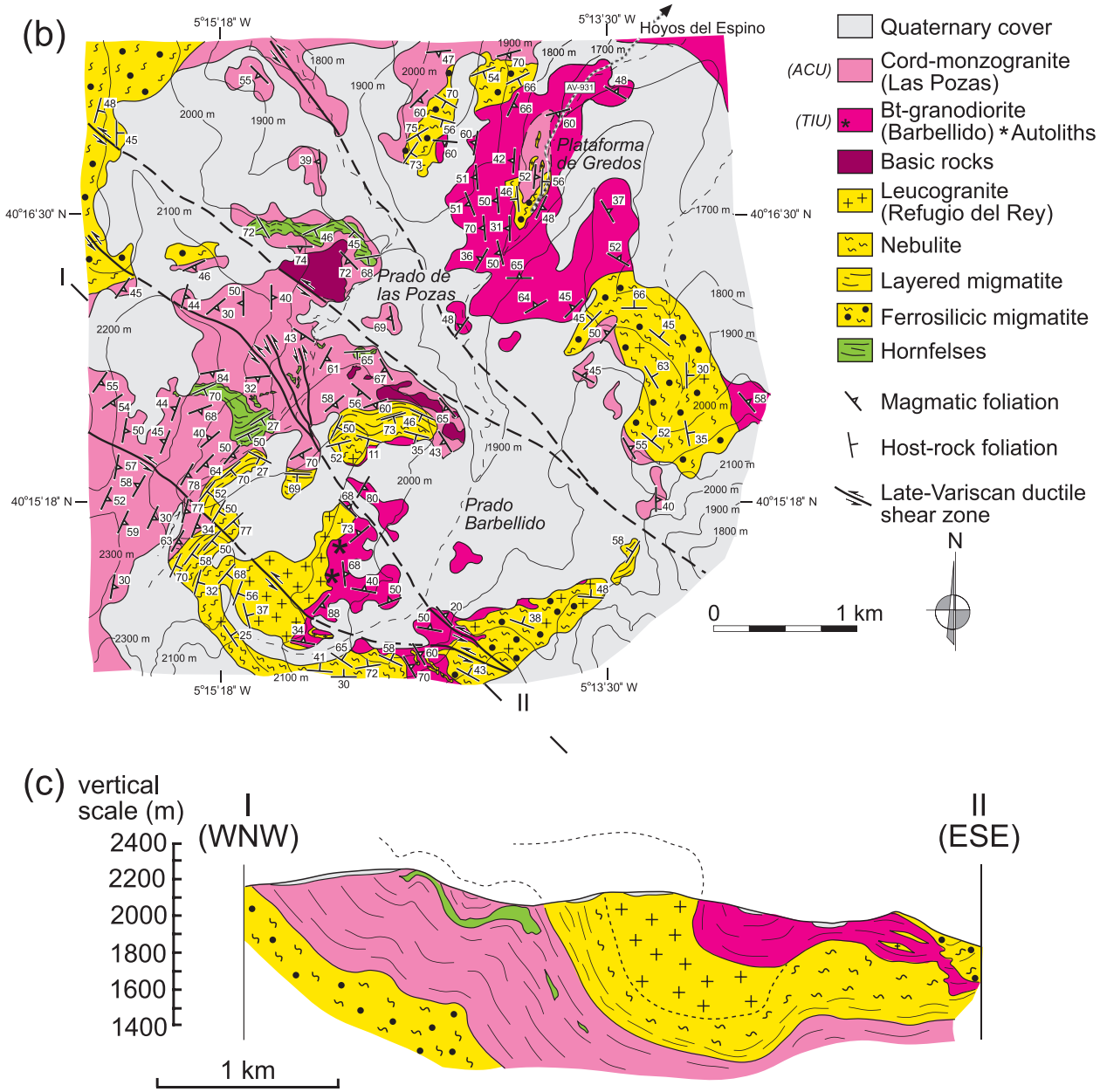

Fig. 1. Continued.

its upper contact (Fig. 3a). In the vicinity of the contacts with pelitic metasediments, the intruding granitoid contains abundant xenoliths of partially digested country rocks (Fig. 3c). Although pelitic xenoliths ranging in size from centimetres to tens of metres are the most abundant, metaquartzites, calc-silicates and fragments of mafic rocks are also present. All these exotic xenoliths represent true 'resisters' that survived digestion by the intruding magma. The Barbellido Bt granodiorite overlies the migmatite–leucogranite layer located at the top of Las Pozas granitoid (Fig. lc). Magma–magma contacts can be seen between the Refugio del Rey leucogranite and the Barbellido Bt granodiorite (Fig. 3d).

For the purpose of this study we have determined the variation in the content of cordierite and K-feldspar in the granitoids, measured at a large number of stations across the mapped area and represented in the form of isocontour lines in Fig. 4. High cordierite volume fractions (8–12%) are observed near the contacts between granitoids and either hornfelses or nebulites (Figs 3e and 4a). In contrast, low volume fractions (<1%) have been measured near the Refugio del Rey leucogranite and its associated leucocratic

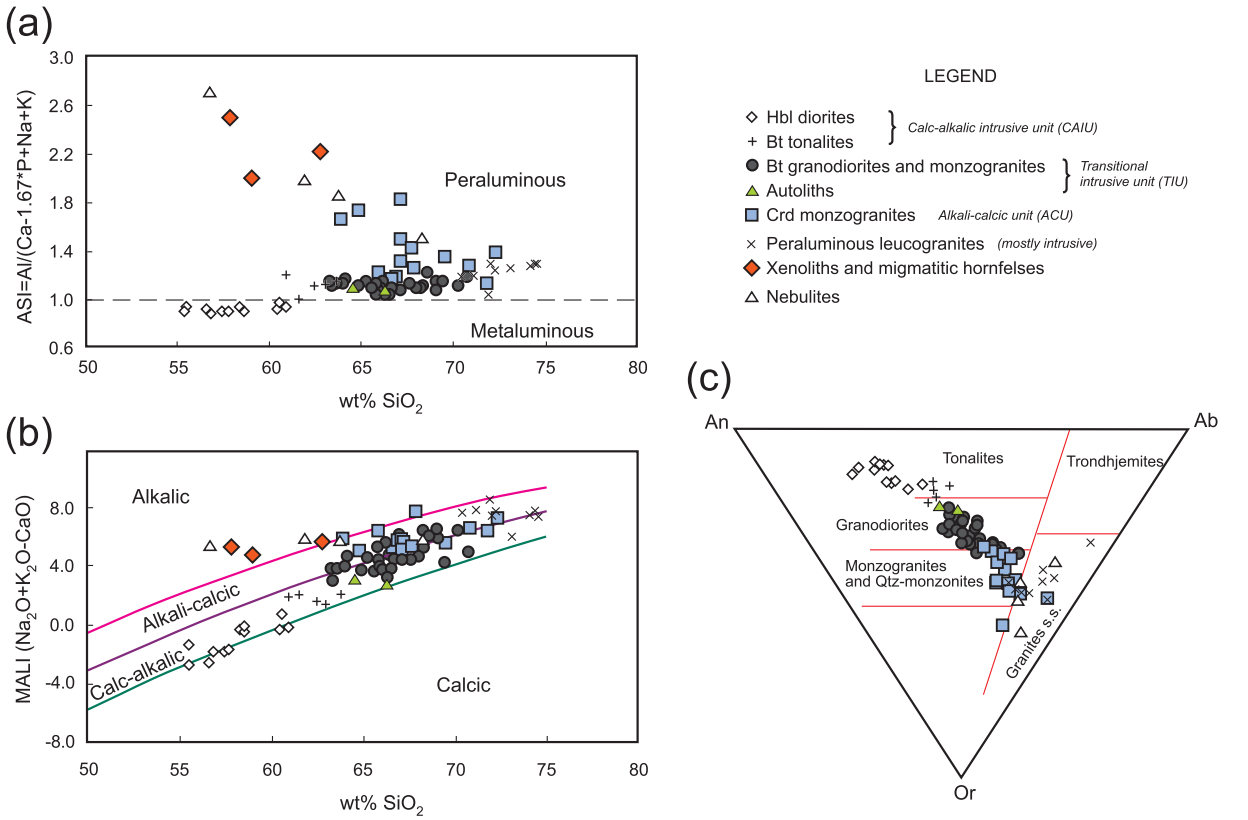

Fig. 2. Granitoid classification diagrams (Frost *et al.*, 2001) (a, b) and O'Connor rock classification triangle (c) for the granitoids of the Gredos Massif. Calc-alkalic and transitional intrusive units (CAIU and TIU) are defined according to the MALI–silica diagram (b). Most Crd monzogranites define an alkali-calcic unit (ACU).

nebulites. The Las Pozas Crd monzogranite has an average volume fraction of cordierite between 4 and 8%, whereas the Crd content in the Barbellido Bt granodiorite is less than 1 vol. %, except for its eastern and northern contacts (Fig. 4a). The contents of Kfs megacrysts show similar patterns to those of cordierite (Fig. 4b), confirming the general observation that cordierite-rich granitoids are also richer in Kfs megacrysts. The sill-like geometry of the intrusive bodies results in large surface areas of mutual contact between the intruding magma and the host-rocks. The granodiorites are mainly intruded subparallel to the main foliation in the hornfelses, although local disruption of the host-rock layering is commonly observed. The result is an intricate geometrical pattern with abundant fragments of hornfels rock partially or totally incorporated into the intruded granitoid mass (Fig. 3c and f).

PETROGRAPHY AND BULK-ROCK COMPOSITIONS

Sampling and analytical techniques

More than 200 samples were collected from the intrusive units and host-rocks over the area mapped in detail (Fig. 1b); of these, 33 samples were chosen for major and trace element analyses. Three samples representative of large intrusive layers were selected for zircon separation and U–Pb dating with SHRIMP. The samples were selected to include all the rock types present in the area. Because this study focuses on the problem of magma–host-rock interaction and the generation of Crd in the alkali-calcic unit (ACU) from the transitional one (TIU), rocks of these groups were preferentially sampled to study the textural and compositional variations. All rocks of these units are coarse-grained and heterogeneous on a scale of several metres. The main heterogeneities are marked by a non-uniform distribution of Crd and Kfs megacrysts. Outcrops with local accumulations of these minerals in bands and/or patches were discarded for sampling. About 5 kg of fresh rock was collected from each outcrop. Samples were crushed and milled to a fine powder in steel cups. Major elements and Zr were analyzed by X-ray fluorescence (XRF) at the University of Oviedo (Spain) using glass beads. The precision of the XRF technique is better than ±1·5 % relative. Trace elements, including rare earth elements (REE), were analyzed by inductively coupled plasma mass spectrometry (ICP-MS)

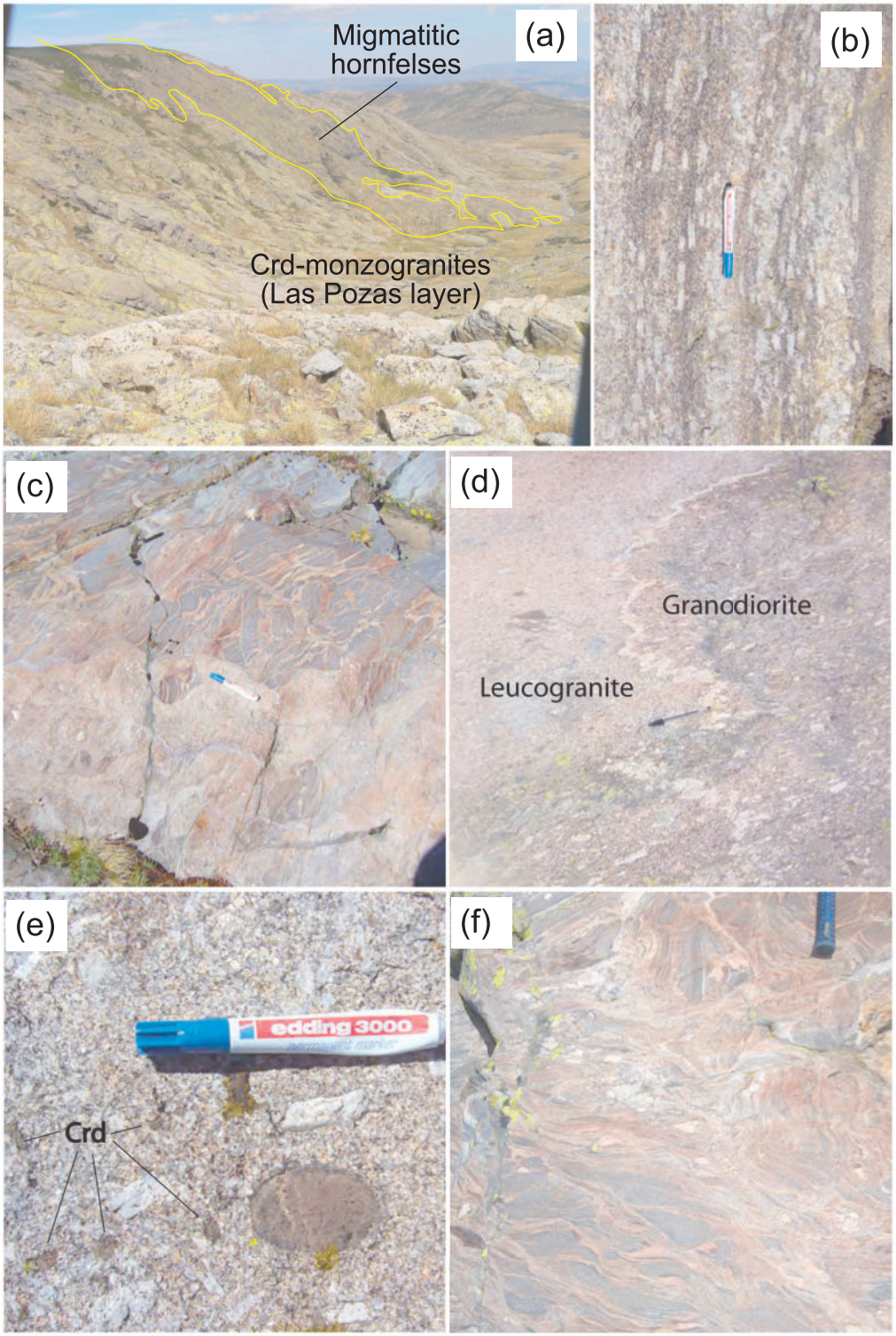

Fig. 3. (a) General view of the Las Pozas Crd monzogranite outcrop, including a large body of migmatitic hornfels. (b) Magmatic foliation in a Crd monzogranite defined by the preferred orientation of Kfs megacrysts. (c) Intrusive contact between the Las Pozas Crd monzogranite and a body of hornfels with small fragments (xenoliths) partially or totally enclosed by the monzogranite. (d) Magma–magma lobate contact between the Barbellido granodiorite (right) and the Refugio del Rey leucogranite (left). (e) Euhedral, rectangular-shaped crystals of Crd in the Las Pozas Crd monzogranite. (f) Network of leucocratic veins pervading a migmatitic hornfels.

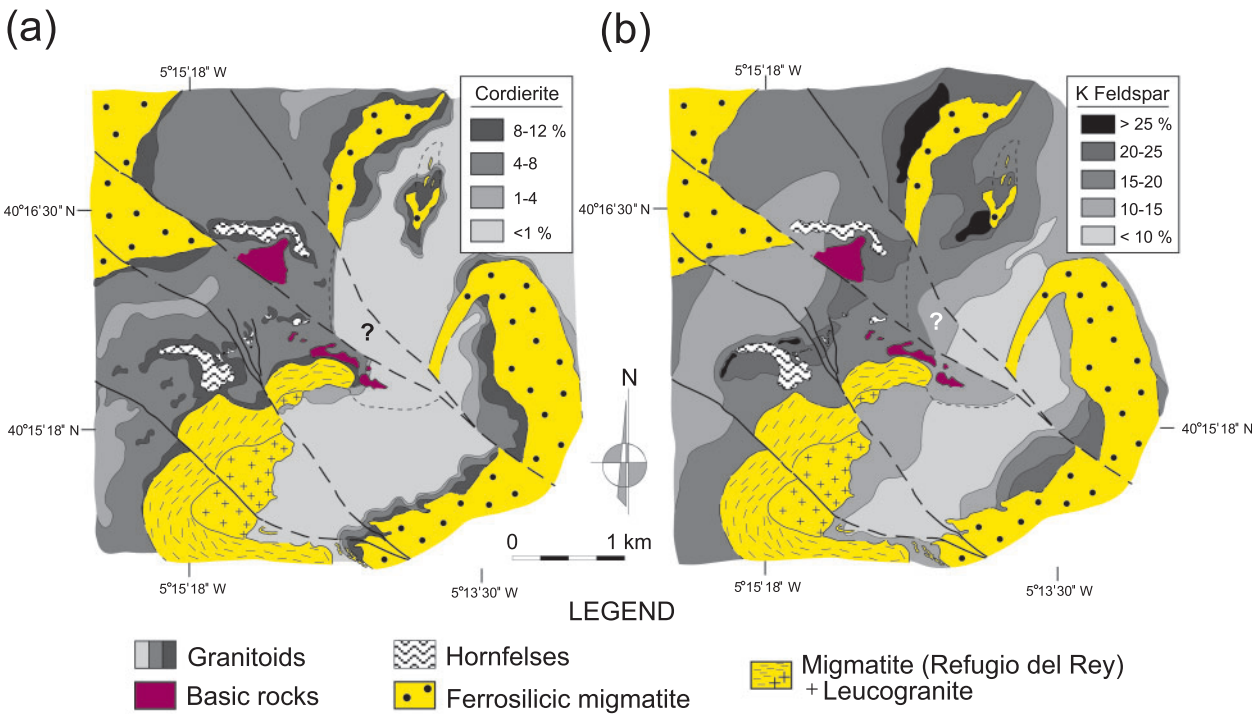

Fig. 4. Isocontour maps representing the volume fractions of cordierite (a) and K-feldspar (b) in the granitoids of the mapped area (Fig. 1b).

with an HP-4500 system at the University of Huelva, following digestion in an $HF + HNO_3$ (8:3) solution, drying and further second dissolution in 3 ml HNO_3. The average precision and accuracy for most of the elements was determined by repeated analyses of the SARM-1 (granite) and SARM-4 (norite) international rock standards, and are in the range 5–10% relative. Electron microprobe analyses were obtained with a JEOL JXA-8200 SuperProbe at the University of Huelva. A combination of silicates and oxides were used for calibration. Both natural rocks and experimental runs were analyzed with the same instrument and using the same protocol for calibration.

PETROGRAPHY

Calc-alkalic and transitional units (Qtz diorites, tonalites, granodiorites and monzogranites)

Granodiorites are by far the most abundant rocks of this intrusive unit. These are coarse-grained, mesocratic rocks. They are commonly porphyritic with large Kfs phenocrysts (up to 10 cm length) heterogeneously distributed in bands and irregular patches. They are composed of Qtz, Pl ($An_{65–32}$), Kfs and Bt. Tonalitic facies lack Kfs phenocrysts and in hand specimen are slightly darker than granodiorites. Plagioclase is characterized in both rock types by complex oscillatory zoning with repeated resorption surfaces and An-rich ($An_{65–60}$) skeletal cores. Biotite in both rock types is similar in composition (Mg-number = 31–40). The Qtz diorites differ in texture and mineralogy. They contain calcic amphibole as either isolated crystals and polycrystalline aggregates or as clots, which show the typical features of amphibole derived from Px reaction in the melt (Castro & Stephens, 1992).

Alkali-calcic unit (Crd-bearing monzogranites)

Rocks of this unit are monzogranites that are characterized by significant heterogeneity, with variations in the content of Crd and Kfs megacrysts (Fig. 4a and b). As described above, these two minerals appear to be particularly concentrated in areas close to the contacts with the country rocks, especially where the intruding granodiorites are in contact with pelitic hornfelses.

Granitoids containing Crd are texturally similar to the Crd-free granodiorites and monzogranites. They have the same grain size, a similar porphyritic character with large Kfs phenocrysts and similar compositions ($An_{50–32}$) and complex zoning patterns in Pl. The Crd monzogranites (ACU) are typically richer in Kfs megacrysts compared with similar rocks of the TIU. Cordierite is usually altered to a fine-grained aggregate of Chl (pinnite) and sericite, always preserving a rectangular prismatic external shape (Fig. 3e), denoting early crystallization in a liquid or low crystal content magma. In places, Sil inclusions are preserved, but no inclusions of other magmatic minerals (e.g. Pl or Bt) have been observed. The Crd crystals are often heterogeneously distributed in the monzogranites in

clusters of a few crystals separated by distances that exceed more than 10 times the average crystal size. In areas of low Crd content (<2 vol. %), large crystals of 4–10 mm length are sparsely distributed in the rock, in places at distances of more than 1 m.

Country rocks and xenoliths: migmatitic hornfelses and migmatites

Migmatitic hornfelses appear as xenoliths on a scale of a few centimetres to tens of metres, hosted by Crd monzogranites (Fig. 3a). The paleosome is formed of fine- to medium-grained metasediment consisting of metagreywacke interbedded with metaquartzite. The metagreywackes are medium- to fine-grained, foliated rocks with a lepidoblastic texture. Their mineral assemblage consists of rounded detrital grains of Qtz, subhedral Bt (Mg-number = 39–48), anhedral grains of Crd (Mg-number = 53–60) with drop-like Qtz, Bt and Zrn inclusions, aligned subhedral Pl grains showing distinctive zonation with cores of andesine to labradorite ($\approx An_{53–39}$) rimmed by andesine to oligoclase ($\approx An_{42–27}$), anhedral Ms, Sil mainly as fibrolite but occasionally as thick prisms, and large prismatic, subhedral grains of And. The main accessory minerals are Tur, Ap and Zrn. Phlebitic hornfelses have trondhjemitic leucosomes aligned parallel to the bedding and collected in shears. Leucosomes of granitic composition are mainly related to agmatites and thick veins rimmed by a Bt melanosome. Some of these leucosomes intrude directly into the Crd monzogranites. The thick leucosome veins are medium- to coarse-grained, leucocratic rocks with allotriomorphic textures. Their mineralogy consists of anhedral Qtz, anhedral to subhedral Kfs, subhedral Pl with cores of andesine to oligoclase ($\approx An_{19–17}$) rimmed by oligoclase to albite ($\approx An_{2–18}$), subhedral Bt (Mg-number = 40), anhedral Ms and subhedral to anhedral Crd (Mg-number = 52–55) that is more ferric than the average Crd of the paleosome (Mg-number = 53–60). Cordierite commonly has inclusions of small, rounded Qtz grains, associated with Zrn grains, and small flakes of Bt. Corroded And grains can occasionally be observed. The accessory mineral assemblage consists mainly of Ap and Zrn.

Two types of migmatite can be distinguished: one is formed of coarse-grained ferrosilicic nebulites, the other is a coarse- to medium-grained layered migmatite underlying the Refugio del Rey leucogranite (Fig. 1b). The coarse-grained ferrosilicic nebulites are mainly melanocratic, heterogeneous rocks showing lamination with bands of felsic nebulite, schlieren of Bt and Kfs augen. Restites, consisting of aggregates of Bt, Crd and Sil, are abundant but heterogeneously distributed. Basic enclaves of quartz-diorite, refractory Qtz-nodules and metaquartzites, and ellipsoidal enclaves of phlebitic migmatite are abundant. Their mineral assemblage consists mainly of anhedral grains of Qtz with undulose extinction, subhedral Bt (Mg-number = 40–48), subhedral grains of Pl that show normal zonation with cores of andesine ($\approx An_{32}$) rimmed by a first band of oligoclase ($\approx An_{21}$) and an outer band of albite ($\approx An_{4}$), subhedral grains of Kfs with perthitic textures, anhedral and subhedral grains of Crd (Mg-number = 60) and Sil. The main accessory minerals are Ilm, Ap, Tur and Zrn. The Refugio del Rey layered migmatites are heterogeneous, coarse- to medium-grained equigranular rocks. Small enclaves hosted in these migmatites are similar to the migmatitic hornfelses. They include metaquartzites and residual refractory aggregates of Bt, Sil and Crd. The mineral assemblage consists of rounded Qtz crystals, subhedral grains of Kfs, subhedral Pl grains showing normal zonation with cores of oligoclase ($\approx An_{16}$) and rims of albite ($\approx An_{3–2}$), subhedral grains of Bt (Mg-number = 36–42) and Crd (Mg-number = 53–54). Cordierite forms subhedral grains usually with abundant, small, drop-like inclusions of Qtz.

Geochemical characteristics

Major elements

The tonalites and granodiorites define coherent and linear geochemical trends for most major elements (Fig. 5). In general, the two units (CAIU and TIU) display good linear trends in silica-variation diagrams for CaO, FeO and MgO over a wide SiO_2 range from 55 to 71 wt %; however, the geochemical link between the Qtz diorites and the other rock types (granodiorites and tonalites) is not straightforward. These relations contrast sharply with the variations displayed by the Crd monzogranites of the ACU. For some oxides (TiO_2, Al_2O_3 and K_2O) they overlap the field of granodiorites and monzogranites of the TIU. They show a flat pattern for CaO with low contents (CaO < 2 wt %) at silica contents of ~65 wt %, for which the CaO content is double in the granodiorites of the TIU. The rocks of the ACU are slightly richer in FeO and MgO and poorer in CaO and Na_2O compared with the granitoids of the TIU at the same silica content. These low-Ca granitoids overlap the xenoliths and nebulites in the CaO, FeO and Na_2O diagrams. Leucogranites plot at the high-silica end of the Harker diagrams (SiO_2 > 70 wt %). No linear array with the other intrusive units is expected; in fact, they display a scattered distribution in these diagrams.

Trace elements

The maximum Sr concentrations (*c.* 300 ppm) are found in the Hbl-diorites of the CAIU, decreasing to about half in the more evolved members of the TIU. The country rocks contain about 100 ppm Sr, which correlates with their low CaO content (<1·5 wt %). A salient feature in terms of trace element abundances is the high Ni content of the country-rock metapelites (about 50 ppm), which contrasts with the low Ni concentration of the more evolved rocks of the TIU. These relationships are illustrated in the

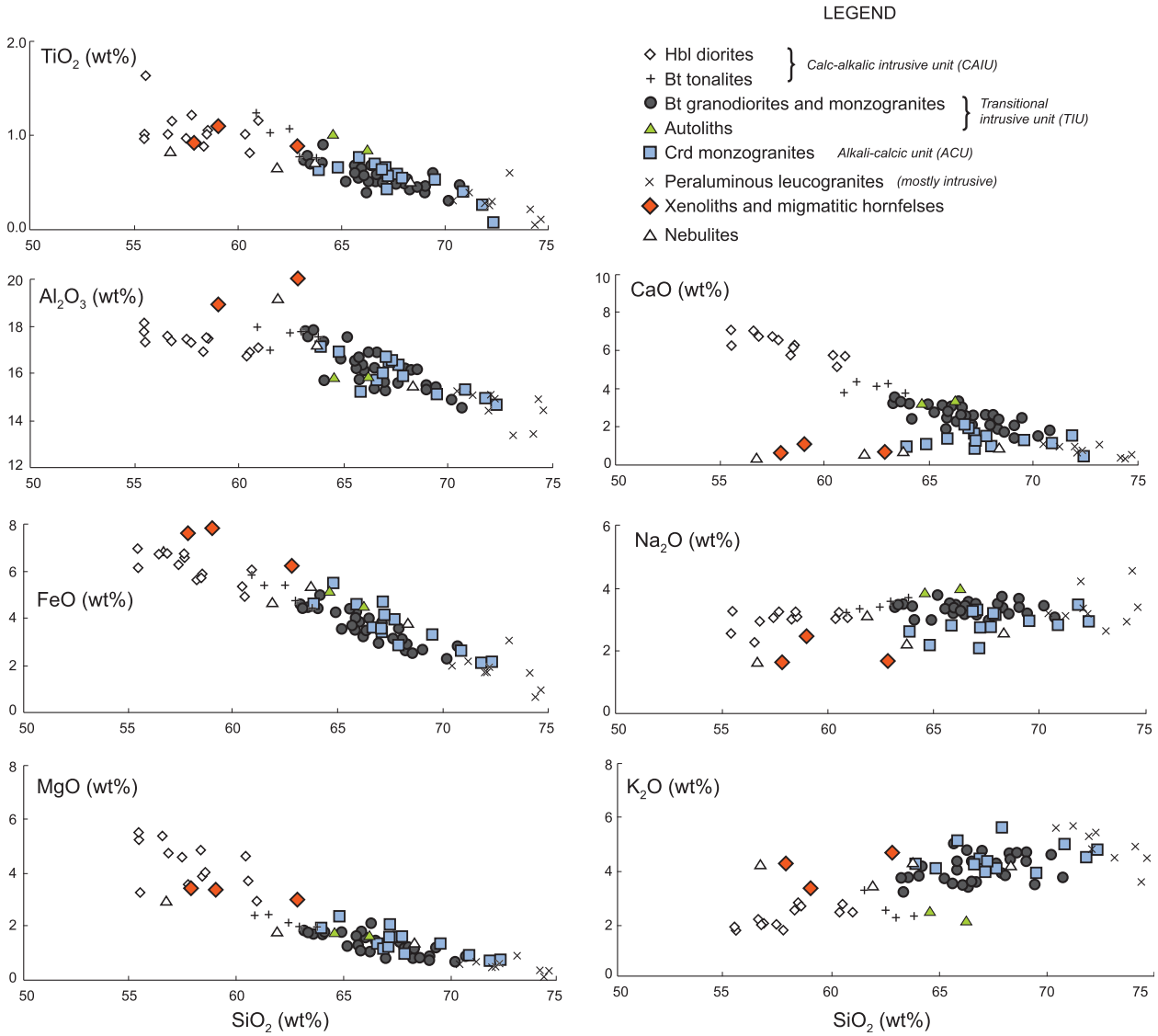

Fig. 5. Major element vs SiO_2 variation diagrams for the intrusive granitoids and country rocks of the Gredos area.

CaO–Ni diagram (Fig. 6a). Independently of the meaning of this CaO–Ni coupled decrease, the point of interest is that the Crd monzogranites (ACU) display a trend of Ni enrichment pointing towards the country-rock metapelites (xenoliths) and nebulites. A similar trend is shown in the Ni–Sr diagram (Fig. 6b), which is not related to magmatic differentiation. Also interesting are the variations in some trace elements with the alumina saturation index [ASI = molar $Al_2O_3/(Na_2O + K_2O + CaO - 1{\cdot}67P_2O_5)$]. There is a marked decrease in Sr and increase in Rb towards the more evolved granodiorites. Two trends, one peraluminous (ASI > 1) and the other metaluminous (ASI < 1) can be identified in the TIU and CAIU respectively (Fig. 6c and e). However, the Crd monzogranites display trends that depart from these magmatic trends and point to the strongly peraluminous field of pelitic metasediments (ASI from 1·5 to 3·0). Finally, departure from magmatic trends is evident in diagrams that can be considered as a proxy of phase equilibria in multisaturated systems. These are, for instance, the CaO vs MgO and molar $K_2O/(K_2O + CaO)$ vs MgO diagrams (Fig. 6d and f). In these diagrams, the CAIU and TIU display good curvilinear trends that follow the evolution of liquid compositions by subtraction of Pl + Hbl or Pl + Cpx. However, there is a clear departure from these ideal cotectic-like trends for the Crd monzogranites.

Intrusive units (calc-alkalic and transitional) are characterized by low Sr/Y ratios (Sr/Y < 10 in Qtz diorites and

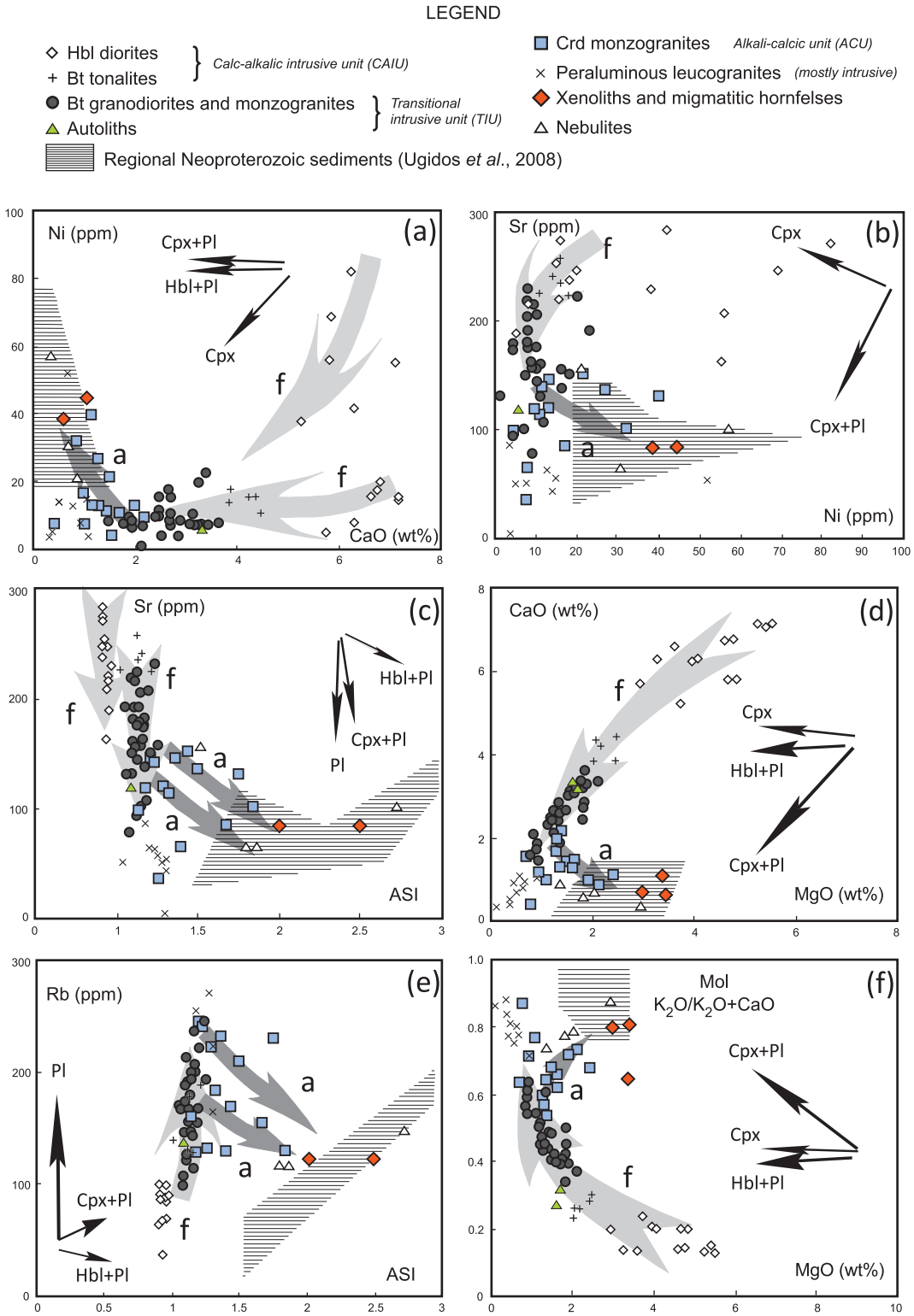

Fig. 6. Major and trace element geochemical variations within the granitoids of the Gredos massif and their associated country rocks. Arrows represent fractionation vectors calculated by assuming constant partitioning over the T range 800–1100°C. This is the range for which the major element abundances have been modelled by using the MELTS algorithm (Ghiorso & Sack, 1995). Partition coefficients used here are: $D_{Sr}^{Cpx}=0{\cdot}08$, $D_{Ni}^{Cpx}=6$, $D_{Rb}^{Cpx}=0{\cdot}02$, $D_{Sr}^{Pl}=1{\cdot}8$, $D_{Rb}^{Pl}=0{\cdot}07$, $D_{Sr}^{Hbl}=0{\cdot}3$, $D_{Ni}^{Hbl}=10$, $D_{Rb}^{Hbl}=0{\cdot}04$ (Philpotts & Schnetzler, 1970). Vectors for joint fractionation of two phases (e.g. Cpx + Pl) are calculated by assuming an average D value with equal and constant proportions of the two minerals. Large grey arrows mark the trends displayed by the intrusive granitoids of the CAIU and TIU groups. In most diagrams, these agree fairly well with the direction of the ideal fractionation vectors, implying the coupled subtraction of Cpx + Pl. It should be noted that the trends defined by the Crd monzogranites (ACU) are transverse to the fractionation vectors. They point to the composition of the host xenoliths and nebulites.

<40 in granodiorites). In the CAIU the low Sr/Y ratios correlate with the slightly fractionated pattern of the REE (Ce/Yb < 6; Fig. 7a). Interestingly, the group of Qtz diorites (CAIU) shows parallel REE patterns with constant Ce/Yb ratios and increasing bulk-rock content of REE with differentiation. The lower values of Yb correspond to the less evolved compositions with Mg-number = 0·60 and Ni = 55 ppm, whereas the higher Yb values belong to rocks with Mg-number = 0·42 and Ni = 8 ppm. Bt granodiorites and tonalites of the TIU show a marked LREE/HREE (light REE to heavy REE) fractionation with Ce/Yb ratios within the range 8–18 (Fig. 7b). There is no correlation between the bulk REE content and Mg-number, silica, or any other differentiation index. The main difference between the two units (CAIU and TIU) are a marked depletion in HREE and a more pronounced Eu anomaly in the TIU (Fig. 7b). The autolith has a central position (Ce/Yb = 15) within the field of Bt granodiorites (Fig. 7b). It can be taken as representative of the average composition of the TIU. The REE patterns of the Crd monzogranites (ACU) are similar to those of the Bt granodiorites. They plot below the average composition represented by the autolith (Fig. 7c). Only one sample is strongly depleted, showing a pattern similar to that of the peraluminous leucogranites of the region (not shown).

ZIRCON GEOCHRONOLOGY AND INHERITANCE

Zircon separation and analytical techniques

Three samples were selected for geochronological studies: a Bt granodiorite far from the contact with the host-rocks (J707-16), a Crd monzogranite near the contact area (J806-3) and a sample of the hornfelses (J707-7); specific locations and chemical composition are given in Table 1. Zircon separation was carried out at Central Services (Huelva University), using standard procedures including magnetic and density separation. At the Research School of Earth Sciences (Australian National University, Canberra), the non-magnetic, heavy minerals concentrate was hand-picked to extract and select zircons on the basis of shape, size and lack of fractures or inclusions. A representative selection was mounted in epoxy resin together with zircon standards SL13 (U = 238) and TEMORA ($^{206}Pb/^{238}U = 0{\cdot}06683$). The mount was polished to expose the grain interiors, photographed at high magnification in transmitted and reflected light, and imaged by scanning electron microscope (SEM) and cathodoluminescence (CL) (Fig. 8) to document the internal growth zoning of the grains. It was then cleaned and coated with high-purity Au in preparation for analysis. Selected areas in zircon grains (spots were chosen to have features as representative as possible of the studied population), were analyzed for U, Th and Pb isotopes on the ANU SHRIMP II ion microprobe using a procedure similar to that described by Williams & Claesson (1987). A 10 kV negative O_2 primary beam was focused to *c.* 20 μm diameter. Positive secondary ions were extracted at 10 kV and mass analyzed at *c.* R5000 on a single ETP multiplier by peak stepping through the isotopes of interest. The U–Th–Pb analyses are reported in Table 2 and plotted on concordia diagrams in Fig. 9. Analytical uncertainties are 1σ precision estimates. All the analyses listed and plotted were corrected for common Pb using the measured ^{204}Pb and a common Pb composition appropriate to the age of each spot (Cumming & Richards, 1975). Uncertainties in the mean ages are 95% confidence limits ($t\sigma$, where t is the Student's t multiplier) and include the uncertainty in the Pb/U calibration (*c.* 0·3–0·5%). Ages were calculated using the constants recommended by the IUGS Subcommission on Geochronology (Steiger & Jäger, 1977).

SHRIMP U–Pb ages and implications

Bt granodiorite (J707-16)

Zircon grains in this sample are mostly euhedral, acicular, with high elongation ratios, parallel banding or concentric oscillatory zoning (less abundant type) (Fig. 8). They lack inherited cores and overgrowths are continuous, displaying only minor local discontinuities in pyramidal terminations. Bt granodiorite $^{206}Pb/^{238}U$ crystallization ages (Table 2) are consistently about 300 Ma, without major radiogenic Pb loss, and Th/U ratios are between 0·04 (dark tip overgrowths) and 0·41 (except spot 1,1 with Th/U = 0·88), providing a concordia age of 302·9 ± 2·5 Ma (MSWD = 1·3) (Fig. 9a). These ages correspond to those estimated for the late granitoids of the Central System batholith.

Crd monzogranite (J806-3)

Zircons in this sample can be divided into two main groups, a first set of euhedral to subhedral elongated zircons with banded parallel zoning or oscillatory concentric continuous overgrowths; and a second group that includes complex anhedral to subhedral crystals, which usually present inherited cores and discontinuous overgrowths (Fig. 8). Excluding analysis 6,1, the simple crystals and growths over inherited cores give a $^{206}Pb/^{238}U$ age of 307·7 ± 3·1 Ma (MSWD = 0·87) for ages over 290 Ma, and 308·2 ± 3·4 (MSWD = 1·3) for ages over 300 Ma (Table 2 and Fig. 9b). As in the sample of the Bt granodiorite, these ages are related to the main age of crystallization of the late granitoids of the Central System batholith. A high percentage of common Pb (14·65) has been measured for spot 5,1, which coincides with an area close to fractures. This explains the aberrant age of 161 ± 2·8 Ma and is consistent with common Pb gain and radiogenic Pb loss. As for the analysis of inherited discontinuous cores and anhedral crystals, these are divided into Neoproterozoic, late Proterozoic and Archaean ages (spots 3,1, 4, 14 and 15,1) and Cambrian ages (spots 1, 8 and 9). The last group of

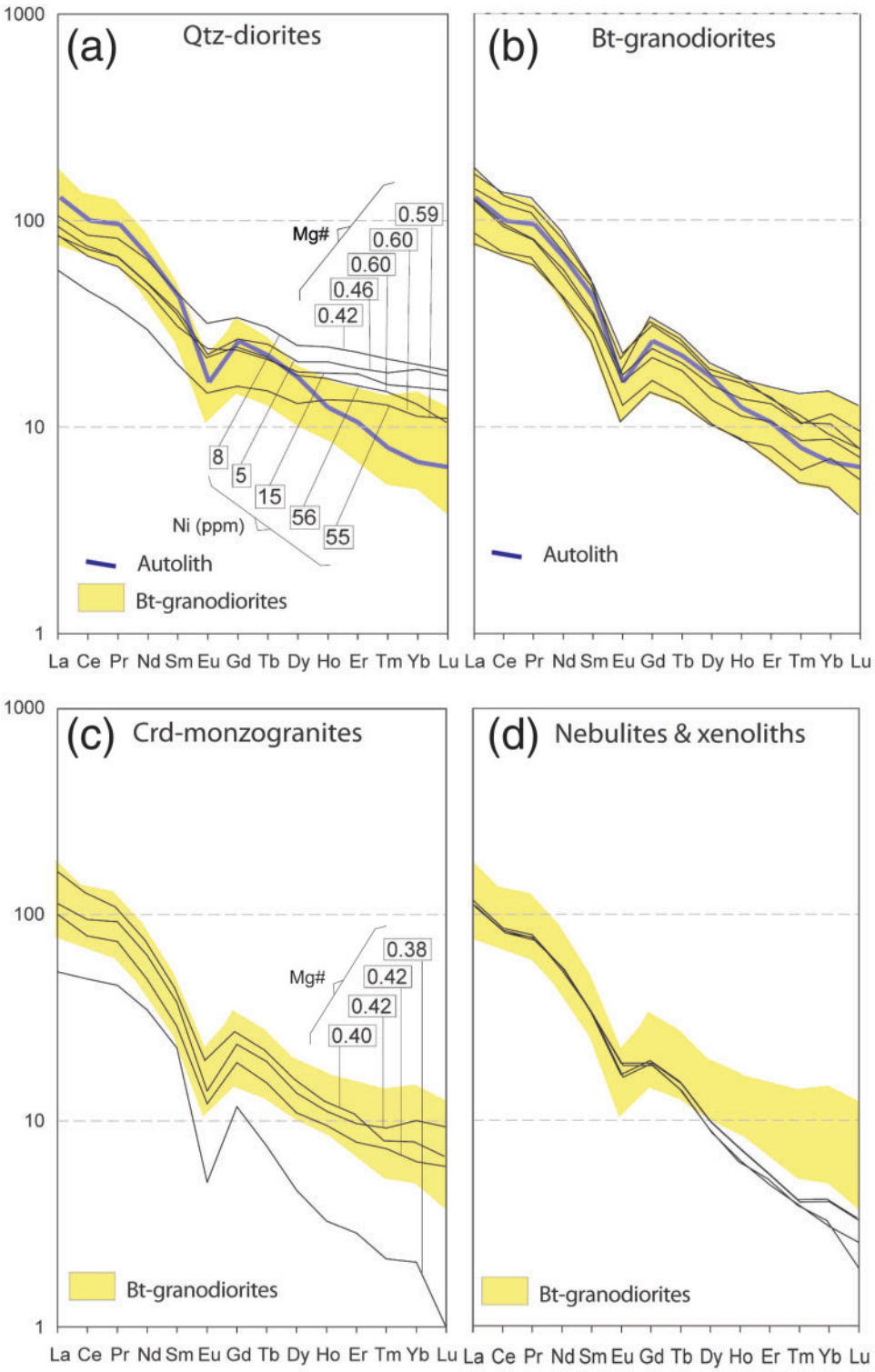

Fig. 7. Chondrite-normalized (Nakamura, 1974) REE diagrams for the intrusive units and country rocks of the Central System batholith in the Gredos area. The field of Bt granodiorites (TIU) is shown in all the diagrams for comparison. Quartz diorites (CAIU) show subparallel REE patterns (a) that correlate fairly well with the bulk-rock Mg-number and Ni content. In contrast, the REE patterns of the intrusive Bt granodiorites (b) show no correlation with any fractionation factor (e.g. Mg-number, not shown). The REE patterns of the Crd monzogranites (c) overlap with the field of the intruding Bt granodiorites and also with the nebulites and xenoliths for LREE; only a slight HREE depletion is observed resulting from assimilation of the HREE-depleted host metasediments (d). Only one sample of Crd monzogranite displays a strongly depleted REE pattern plotting below the general trend.

Table 1: Representative whole-rock compositions of granitoids and host-rocks of the Gredos Massif

Unit:	Calc-alkalic intrusive unit (CAIU)							Transitional intrusive unit (TIU)								
Rock type:	Hbl diorites						Bt tonalites	Bt granodiorites and monzogranites								
Sample:	M330*	M424*	M660A*	M670*	M799*	J809-13	M801*	J809-1	M647A*	J809-7	J709-1	A809-4A	A809-3	J-707-16	M681A*	J-706-47	M175*
wt %																	
SiO_2	60·34	60·89	55·40	55·47	56·53	61·05	61·48	62·14	63·28	64·07	65·69	65·77	66·45	66·92	67·59	68·19	68·24
TiO_2	1·00	1·14	0·96	1·60	1·00	1·15	1·01	0·89	0·78	0·89	0·61	0·76	0·68	0·50	0·49	0·44	0·45
Al_2O_3	16·79	17·13	18·14	17·35	17·63	17·64	17·02	17·14	17·61	15·74	16·27	15·79	15·42	15·7	15·66	16·05	16·21
FeO_t	5·42	6·12	6·21	8·10	6·79	5·75	5·49	5·14	4·56	5·05	3·76	4·35	4·08	3·05	3·22	2·69	2·98
MgO	4·66	2·93	5·23	3·26	5·40	2·21	2·48	1·70	1·83	1·80	0·33	1·83	1·41	0·85	1·47	0·88	1·19
MnO	0·09	0·12	0·12	0·15	0·13	0·08	0·08	0·10	0·07	0·07	0·04	0·07	0·06	0·05	0·06	0·03	0·05
CaO	5·80	5·73	7·15	6·29	7·09	4·44	4·45	3·24	3·63	2·45	1·92	2·87	2·68	2·13	2·66	1·91	2·44
Na_2O	3·07	3·09	2·57	3·27	2·29	3·24	3·35	3·58	3·47	3·01	3·49	3·23	3·22	3·48	3·00	3·72	3·39
K_2O	2·49	2·46	1·91	1·74	2·18	2·29	3·29	3·94	3·22	4·19	5·06	4·08	4·36	4·77	4·28	4·69	4·41
P_2O_5	0·33	0·16	0·17	0·38	0·14	0·25	0·29	0·52	0·32	0·50	0·44	0·24	0·27	0·36	0·65	0·14	0·28
LOI	0·97	0·61	1·15	1·76	1·18	0·81	0·97	0·81	0·84	1·32	0·71	0·56	0·67	1·26	0·78	0·64	0·59
Total	101·0	100·4	99·01	99·54	100·4	99·62	99·91	99·82	100·4	99·71	99·77	100·1	99·80	99·07	99·88	99·38	100·3
ppm																	
V	104·5	128·8	119·9	130·2	161·8	81·45		52·59	57·08	60·88	43·22	43·67	60·33		42·83		36·92
Cr	207·2	61·72	286·00	211·2	809·3	132·4		92·34	163·7	166·8	138·1	97·47	167·3		153·9		64·96
Ni	56·13	5·20	15·66	8·10	55·39	7·05		6·82	8·15	11·71	7·01	8·82	10·94		8·86		10·28
Rb	100·8	100	85·22	69·93	36·88	81·88		164·8	147·2	156·4	201·7	101·1	169·7		145·2		169·1
Sr	208·2	189·4	221·00	216·2	163·4	260·5		103·1	177·1	108·2	102·5	79·35	132·5		158·7		145·2
Y	23·55	29·23	26·16	33·41	18·99	12·17		7·18	22·50	20·45	10·50	10·38	22·26		20·13		16·44
Zr	117·2	125·8	158·1	92·84	97·88	210·4		317·6	145·7	321·9	114·3	212·3	218·9		108·5		129·2
Nb	10·15	11·60	6·74	14·06	4·08	9·35		12·88	15·16	16·53	13·02	8·34	13·71		12·43		12·74
Ba	363·3	414·7	287·1	314·8	188·8	589·8		398·6	460·1	445·2	330·6	285·9	669·4		462·4		398·2
La	22·23	20	20·15	24·59	13·62	30·14		15·76	42·52	39·35	20·25	18·28	33·31		29·94		29·67
Ce	45·50	44·52	41·15	51·63	27·96	57·48		32·41	80·57	81·76	42·09	41·31	71·53		58·98		57·02
Pr	6·15	6·18	5·56	7·55	3·49	8·15		4·90	10·74	11·66	5·97	5·62	9·83		7·52		7·46
Nd	22·42	22·68	20·63	29·35	13·45	27·18		17·46	36·89	39·59	19·29	19·42	32·11		26·41		24·64
Sm	5·16	5·39	4·53	6·59	2·98	5·58		3·09	7·30	7·53	3·76	4·24	7·02		5·25		5·10
Eu	1·20	1·27	1·35	1·78	0·82	1·46		0·94	1·28	1·01	0·58	0·72	1·17		1·01		0·93
Gd	4·79	5·31	4·69	6·67	3·11	4·58		2·77	6·15	6·61	2·86	3·34	6·27		4·75		4·30
Tb	0·78	0·91	0·77	1·09	0·54	0·71		0·35	0·90	0·99	0·46	0·50	0·94		0·73		0·67
Dy	4·30	5·10	4·55	6·06	3·18	3·27		1·66	4·38	4·90	2·46	2·54	4·56		3·90		3·33
Ho	0·92	1·13	0·99	1·32	0·73	0·54		0·31	0·89	0·93	0·47	0·47	0·91		0·74		0·62
Er	2·50	3·09	2·90	3·66	2·12	1·33		0·82	2·22	2·16	1·10	1·28	2·44		2·07		1·70
Tm	0·36	0·45	0·40	0·52	0·31	0·15		0·08	0·26	0·28	0·13	0·15	0·35		0·26		0·21
Yb	2·05	3·06	2·51	3·21	1·80	0·79		0·46	1·66	1·45	0·80	1·13	2·34		1·86		1·40
Lu	0·26	0·43	0·37	0·46	0·27	0·10		0·09	0·19	0·19	0·09	0·14	0·31		0·23		0·17
Hf	3·03	3·79	3·92	2·65	2·83	2·76		3·47	3·96	3·14	1·47	1·37	3·16		3·12		3·80
Ta	1·28	1·86	0·86	1·12	0·66	1·06		1·82	0·82	1·69	2·38	1·09	3·16		1·46		1·05
W	1·96	2·91	1·04	1·35	0·22	0·63		1·88	1·45	1·17	2·20	0·58	0·95		1·27		3·77
Pb	16·96	21·82	15·21	18·01	10·16	14·13		13·82	110·7	19·36	18·09	14·18	22·62		29·62		31·91
Th	7·30	5·16	6·28	6·52	3·80	9·73		3·68	15·92	21·69	10·27	10·59	15·32		11·95		14·16
U	2·15	4·86	2·22	2·23	0·89	1·50		6·17	4·09	3·70	3·72	2·50	5·13		3·31		2·16

(continued)

Table 1: Continued

Unit:	Transitional intrusive unit (TIU)			Alkali-calcic unit (ACU)					Host rocks							
Rock type:		Autoliths		Crd monzogranites					Leucogr.	Nebulites		Xenoliths				
Sample:	J-806-1	J809-6	RR-4	J-806-3	M783*	J809-5	J809-16	J808-109	J-806-4	J809-10	J-706-43	J-707-7	J709-2	J809-11A	J-707-7	J606-15
wt %																
SiO_2	68·97	66·24	64·58	65·80	67·64	63·84	66·58	67·86	74·11	63·74	68·31	56·69	57·84	58·98	61·86	62·79
TiO_2	0·46	0·84	1·00	0·76	0·58	0·64	0·70	0·54	0·22	0·72	0·50	0·81	0·91	1·07	0·65	0·86
Al_2O_3	15·42	15·83	15·82	15·25	16·39	17·19	15·71	15·92	13·46	17·23	15·51	21·03	20·45	18·92	19·21	20·00
FeO_t	2·80	4·48	5·13	4·62	4·00	4·64	3·69	3·08	1·71	5·41	3·85	6·88	7·65	7·87	4·71	6·27
MgO	0·91	1·61	1·70	1·48	1·63	1·90	1·37	1·07	0·37	2·03	1·37	2·95	3·44	3·36	1·83	2·98
MnO	0·05	0·05	0·06	0·05	0·06	0·08	0·07	0·03	0·02	0·07	0·06	0·08	0·16	0·10	0·06	0·08
CaO	1·47	3·31	3·15	1·43	1·49	0·97	2·16	0·99	0·39	0·69	0·87	0·35	0·60	1·08	0·58	0·69
Na_2O	3·67	3·98	3·84	2·80	2·78	2·64	3·24	3·15	2·93	2·23	2·58	1·65	1·64	2·47	3·13	1·68
K_2O	4·40	2·09	2·49	5·09	4·10	4·25	4·26	5·61	4·86	4·30	4·19	4·21	4·25	3·32	3·44	4·65
P_2O_5	0·19	0·28	0·34	0·20	0·27	0·33	0·43	0·35	0·22	0·29	0·12	0·16	0·17	0·15	0·24	0·18
LOI	0·91	0·63	0·86	1·45	1·26	2·25	0·96	0·91	1·09	2·32	1·48	3·92	1·76	1·74	3·26	3·72
Total	99·25	99·89	98·97	98·93	100·2	99·29	99·62	99·89	99·38	99·68	98·84	98·73	99·81	100·1	98·97	98·00
ppm																
V		48·08			58·50	65·10	48·29	24·89		69·52			84·03	118·6		
Cr		91·89			158·5	192·2	115·2	94·07		151·7			112·3	152·4		
Ni		5·84			21·48	16·99	9·56	7·43		30·69			38·40	44·65		
Rb		137·6			170·1	156·2	130·1	132·6		116·9			121·8	123·9		
Sr		119·1			152·6	85·46	119·4	36·79		65·17			83·57	83·65		
Y		15·71			18·34	11·94	13·60	4·16		8·26			7·89	7·02		
Zr		282·4			90·26	174·9	214·1	189·8		238·7			180·9	222·3		
Nb		15·65			14·67	11·73	10·70	9·97		9·50			10·61	11·03		
Ba		172			454·1	311·7	341·2	174·6		320·3			488·8	393·6		
La		30·31			38·41	23·82	26·89	12·51		25·81			27·02	26·15		
Ce		60·56			76·46	48·3	58·22	29·89		50·10			51·37	50·20		
Pr		8·77			9·88	6·88	8·59	4·22		6·99			7·22	7·16		
Nd		29·85			33·59	22·22	29·02	15·77		24·81			23·85	24·52		
Sm		6·16			6·37	4·26	5·55	3·34		4·80			4·88	4·78		
Eu		0·91			1·08	0·68	0·79	0·28		0·91			1·04	1·04		
Gd		5·11			5·26	3·81	4·68	2·33		3·78			3·68	3·68		
Tb		0·78			0·78	0·55	0·70	0·27		0·54			0·50	0·50		
Dy		4·16			3·82	2·69	3·36	1·13		2·40			2·18	2·16		
Ho		0·66			0·66	0·52	0·61	0·18		0·39			0·33	0·34		
Er		1·65			1·69	1·26	1·55	0·46		0·87			0·80	0·77		
Tm		0·19			0·19	0·18	0·23	0·05		0·10			0·09	0·09		
Yb		1·06			1·24	1·02	1·62	0·33		0·65			0·51	0·49		
Lu		0·15			0·16	0·15	0·23	0·02		0·08			0·05	0·06		
Hf		2·73			2·58	2·09	3·04	1·70		2·18			0·87	1·68		
Ta		3·32			1·58	2·39	1·50	1·15		1·01			1·26	0·94		
W		0·73			1·52	2·11	1·51	0·54		2·34			0·70	1·14		
Pb		12·62			27·16	20·62	20·08	14·17		17·02			18·67	15·64		
Th		15·12			16·69	12·56	18·16	12·77		10·36			10·31	9·71		
U		2·73			6·34	5·04	6·23	3·23		5·06			2·76	2·33		

*Samples from Moreno-Ventas (1991) re-analyzed for this study.
Leucogr., leucogranites.

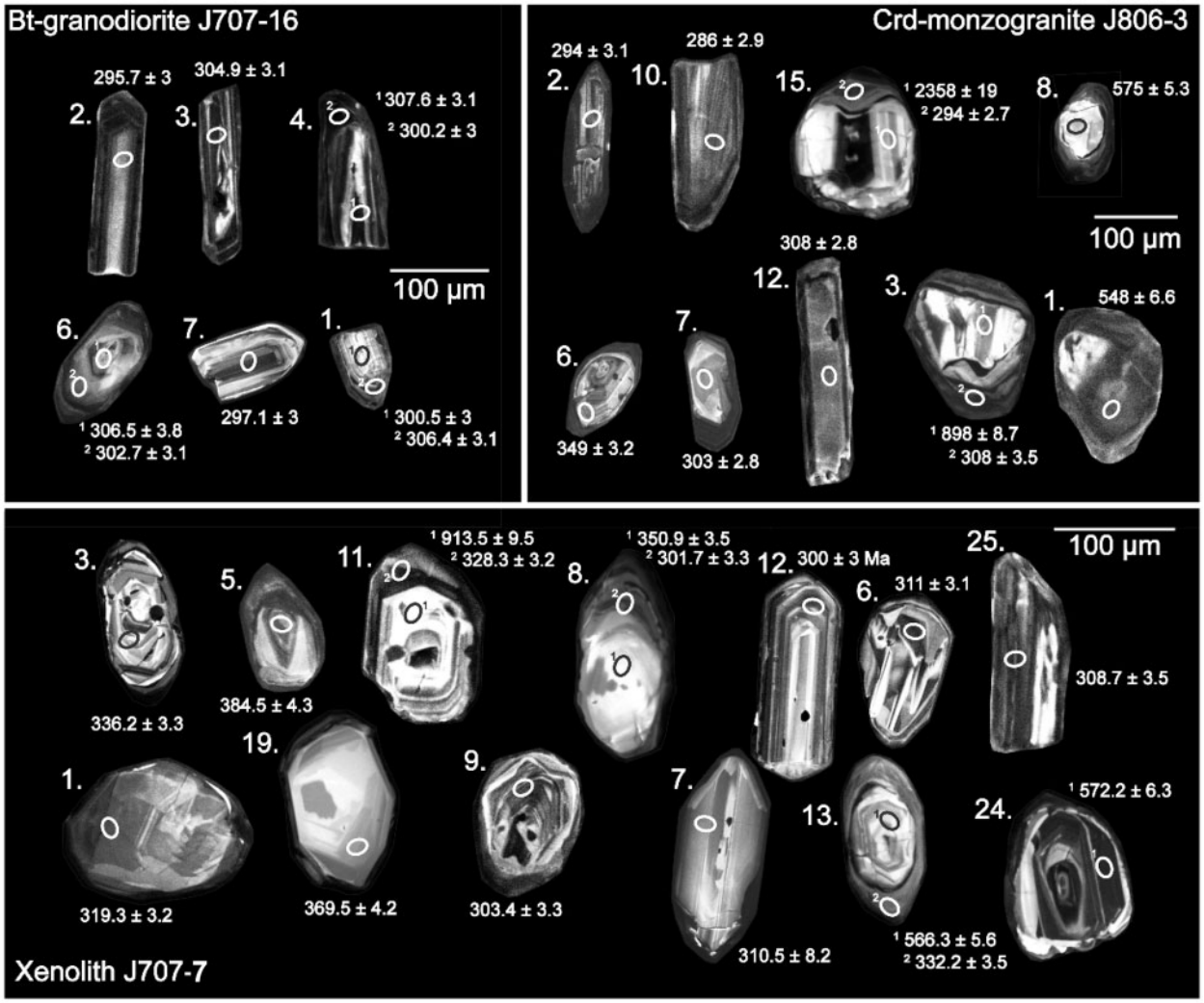

Fig. 8. Cathodoluminescence images of a representative selection of the analyzed zircons from the three samples chosen for the ion microprobe U–Th–Pb study. Zircon number, location of the SHRIMP spots and their resulting $^{206}Pb/^{238}U$ ages (Ma) are indicated. Data are given in Table 2.

ages corresponds to that obtained from the metasediments and inherited zircons previously studied in the Central System batholith (Bea *et al.*, 2003; Zeck *et al.*, 2004; Castiñeiras *et al.*, 2008).

Xenolith (J707-7)

Almost all zircons in this sample are anhedral or complex crystals, with an inherited core discontinuously surrounded by an oscillatory overgrowth, although crystals with continuous oscillatory zoning are also present (Fig. 8). The proportion of simple prismatic and elongated zircons is lower. Some zircons have extreme U concentrations over 1%. Many have central core-like zones with lower U contents. Some of these are clearly inherited cores, although they are not always easily discernible. Inherited ages and analyses with >2500 ppm of U have been excluded to determine a concordia age for this sample (Fig. 9c), because of the dispute over their origin (McLaren *et al.*, 1994; Wingate *et al.*, 1998; Hoskin & Black, 2000; Zeck & Whitehouse, 2002). Analyses with Th/U ratios below 0·1 do not coincide with a single age group, but are present in the various age groups found (spots 1,1, 22,1 and 20,2, Table 2), and are consistent with the ages of other spots with lower U contents (spots 18,1, 5,1 and 27,2, Table 2). Therefore, the use of these data with low Th/U ratios does not modify the pattern of the relative probability histograms. The concordia age for the data used is 303·6 ± 2·5 Ma (MSWD = 0·96) (Fig. 9c). The relative probability histogram (Fig. 9d) for the xenolith sample shows a main peak at around 305 Ma that agrees

Table 2: Summary of SHRIMP U–Pb zircon data

Grain and spot	^{206}Pb (ppm)	$^{206}Pb_c$ %	^{238}U (ppm)	^{232}Th (ppm)	Th/U	$^{204}Pb/^{206}Pb$	± %	$^{206}Pb/^{238}U$	± %	$^{207}Pb/^{235}U$	± %	$^{207}Pb/^{206}Pb$	± %	$^{206}Pb/^{238}U$ age (Ma)	±	$^{207}Pb/^{206}Pb$ age (Ma)	±
Sample J707-16																	
Simple crystals (mainly euhedral), concordant cores and overgrowths																	
1,1	159	0·31	3867	3276	0·88	0·000169	9	0·04772	1·0	0·3445	1·3	0·05236	0·82	300·5	3	301	19
1,2	80·4	0·82	1907	575	0·31	0·000449	8	0·04868	1·0	0·3494	1·7	0·05204	1·40	306·4	3·1	287	31
2,1	107	0·09	2645	909	0·36	0·000047	21	0·04695	1·0	0·3475	1·2	0·05244	0·49	295·7	3	304	11
3,1	56·4	0·02	1356	46	0·04	0·000010	106	0·04844	1·0	0·3549	1·3	0·05202	0·63	304·9	3·1	286	14
4,1	83·5	0·02	1989	122	0·06	0·000011	54	0·04887	1·0	0·3468	1·2	0·05267	0·76	307·6	3·1	315	17
4,2	62·3	0·04	1521	89	0·06	0·000024	49	0·04767	1·0	0·3394	1·2	0·05276	0·62	300·2	3	319	14
5,1	5·3	0·00	122	49	0·41	0·000018	66	0·05068	1·3	0·3794	2·2	0·05429	1·80	318·7	4	383	41
5,2	109	0·00	2621	64	0·03	0·000001	263	0·04840	1·0	0·3523	1·1	0·05279	0·41	304·7	3	320	9·3
6,1	6·3	0·00	151	60	0·41			0·04869	1·3	0·3577	2·1	0·05328	1·70	306·5	3·8	341	38
6,2	54·4	0·39	1312	90	0·07	0·000214	20	0·04808	1·0	0·3484	1·7	0·05255	1·40	302·7	3·1	309	32
7,1	34	0·06	839	125	0·15	0·000036	39	0·04717	1·0	0·3376	1·3	0·05191	0·81	297·1	3	281	19
Sample J806-3																	
Discordant cores and anhedral crystals																	
1,1	96·2	3·22	1222	479	0·41	0·001805	20	0·0887	1·3	0·72	11	0·0589	11	548	6·6	564	240
3,1	189	0·03	1469	655	0·46	0·000018	36	0·1495	1·0	1·46	1·2	0·0706	0·6	898	8·7	946	12
4,1	129	0·09	825	70	0·09	0·000056	24	0·1818	0·9	3·40	1·1	0·1356	0·6	1077	9·3	2171	11
5,1	9·87	14·65	389	54	0·14	0·007938	6	0·0252	1·8	0·20	19	0·0570	19	161	2·8	480	430
8,1	50	0·05	624	490	0·81	0·000026	65	0·0933	1·0	0·77	1·2	0·0600	0·7	575	5·3	604	15
9,1	369	1·21	5025	836	0·17	0·000676	6	0·0845	1·0	0·69	2	0·0590	1·7	523	4·6	568	38
14,1	92·5	0·02	249	312	1·30	0·000147	38	0·4327	1·0	9·51	1	0·1593	0·3	2318	19	2448	5
15,1	165	0·00	434	101	0·24	0·000017	59	0·4417	1·0	9·12	1·7	0·1497	1·4	2358	19	2343	24
Simple crystals (mainly euhedral) and overgrowths																	
2,1	10·5	0·14	262	228	0·90	0·000078	63	0·0467	1·1	0·34	2·2	0·0528	1·9	294	3·1	321	43
3,2	134	0·38	3169	57	0·02	0·000208	10	0·0489	1·1	0·36	1·4	0·0527	0·8	308	3·5	314	18
4,2	154	0·01	603	152	0·26	0·000002	97	0·2968	0·9	4·94	1	0·1207	0·3	1676	14	1967	5
5,2	237	0·82	5504	83	0·02	0·000449	5	0·0498	0·9	0·35	1·4	0·0522	1·1	313	2·8	295	25
6,1	71·6	1·64	1474	109	0·08	0·000901	7	0·0556	1·0	0·43	2·6	0·0556	2·4	349	3·2	435	53
7,1	61·6	0·05	1490	202	0·14	0·000029	58	0·0481	1·0	0·35	1·2	0·0524	0·8	303	2·8	303	17
10,1	26·7	0·27	684	248	0·37			0·0454	1·0	0·33	2·1	0·0521	1·8	286	2·9	291	41
12,1	54	0·03	1285	179	0·14	0·000302	12	0·0489	0·9	0·36	1·1	0·0529	0·6	308	2·8	322	15
15,2	62·9	0·55	1562	8	0·01	0·000010	59	0·0466	0·9	0·34	1·7	0·0525	1·4	294	2·7	305	31
Sample J707-7																	
Discordant cores and anhedral crystals																	
1,1	320	0·11	7323	13	0·020	0·000059	30	0·05078	1·0	0·368	1·3	0·05345	0·53	319·3	3·2	311	17
5,1	66·7	0·57	1255	236	0·194	0·000315	12	0·06146	1·2	0·465	1·7	0·05947	0·56	384·5	4·3	407	29
6,1	85·2	0·00	2006	18	0·009			0·04943	1·0	0·357	1·2	0·05230	0·55	311·0	3·1	299	12
19,1	11·3	1·21	219	68	0·320	0·000666	23	0·05899	1·2	0·514	4·1	0·07281	1·30	369·5	4·2	714	84
20,1	267	0·18	812	100	0·127	0·000121	9	0·38160	1·2	9·120	1·2	0·17489	0·23	2084	20	2590	4
22,1	566	0·37	10166	93	0·009	0·000205	6	0·06462	1·2	0·466	1·3	0·05535	0·21	403·6	4·5	300	12
24,1	42·9	0·00	539	54	0·104	0·000039	41	0·09280	1·2	0·771	1·4	0·05965	0·76	572·2	6·3	612	18
Simple crystals (mainly euhedral), concordant cores and overgrowths																	
2,1	28·5	1·46	734	212	0·297	0·000797	11	0·04451	1·6	0·316	3·5	0·06311	0·84	280·7	4·3	260	71
3,1	192	0·01	4172	90	0·022	0·000006	71	0·05354	1·0	0·388	1·1	0·05267	0·36	336·2	3·3	311	9
4,1	72·9	2·14	1519	259	0·176	0·001176	22	0·05470	3·5	1·031	36	0·15200	31·0	343·0	12	2186	620

(continued)

Table 2: Continued

Grain and spot	^{206}Pb (ppm)	$^{206}Pb_c$ %	^{238}U (ppm)	^{232}Th (ppm)	Th/U	$^{204}Pb/^{206}Pb$	± %	$^{206}Pb/^{238}U$	± %	$^{207}Pb/^{235}U$	± %	$^{207}Pb/^{206}Pb$	± %	$^{206}Pb/^{238}U$ age (Ma)	±	$^{207}Pb/^{206}Pb$ age (Ma)	±
7,1	139	7·79	3014	387	0·133	0·004275	3	0·04930	2·7	0·296	24	0·10690	8·20	310·5	8·2	−135	590
8,1	237	0·90	4880	31	0·006	0·000495	5	0·05595	1·0	0·411	1·5	0·06058	0·48	350·9	3·5	343	27
8,2	14·5	0·32	350	210	0·620	0·000176	37	0·04791	1·1	0·345	2·6	0·05477	1·30	301·7	3·3	294	53
9,1	86·7	0·74	2079	36	0·020	0·000403	9	0·04820	1·1	0·341	1·8	0·05723	0·51	303·4	3·3	255	32
10,1	35·3	1·03	858	713	0·858	0·000567	12	0·04739	1·1	0·345	2·6	0·06115	0·75	298·5	3·1	323	53
11,1	27·5	0·13	210	417	2·053	0·000077	41	0·15220	1·1	1·504	1·7	0·07274	1·10	913·5	9·5	976	27
11,2	152	0·24	3373	9	0·003	0·000133	12	0·05225	1·0	0·377	1·2	0·05425	0·36	328·3	3·2	299	15
12,1	57·7	0·34	1403	678	0·499	0·000187	18	0·04766	1·0	0·343	1·6	0·05493	0·62	300·1	3·0	294	27
13,1	48·5	0·44	612	235	0·398	0·000245	16	0·09183	1·0	0·742	1·6	0·06214	0·63	566·3	5·6	552	28
13,2	80·5	0·58	1761	43	0·025	0·000317	11	0·05289	1·1	0·392	1·6	0·05812	0·50	332·2	3·5	349	27
14,1	28·4	0·44	687	386	0·581	0·000243	23	0·04792	1·1	0·334	2·2	0·05417	0·88	301·8	3·1	222	44
15,1	21·1	0·25	533	284	0·550	0·000138	46	0·04589	1·1	0·328	2·3	0·05393	0·94	289·2	3·1	281	47
16,1	51·3	0·64	1228	185	0·156	0·000350	21	0·04837	1·0	0·340	2·5	0·05617	0·72	304·5	3·1	243	53
17,1	46·6	0·41	1135	446	0·406	0·000227	21	0·04760	1·0	0·347	2·6	0·05620	1·80	299·8	3·0	326	54
18,1	150	0·60	3435	4481	1·350	0·000328	28	0·05049	1·1	0·367	3·5	0·05760	1·90	317·5	3·5	319	76
20,2	482	7·68	11259	87	0·008	0·004205	5	0·04597	1·6	0·318	11	0·11200	1·50	289·7	4·4	203	260
21,1	333	0·30	7619	30	0·004	0·000162	25	0·05078	1·0	0·370	1·8	0·05518	0·95	319·3	3·1	320	34
22,2	18·5	0·23	444	233	0·543	0·000124	53	0·04834	1·2	0·374	2·5	0·05394	1·10	304·3	3·5	291	50
23,1	25	1·93	588	147	0·258	0·001060	12	0·04846	1·2	0·353	4·2	0·06834	0·94	305·0	3·5	321	92
25,1	17·5	0·37	415	239	0·595	0·000202	35	0·04906	1·2	0·345	2·6	0·05402	1·10	308·7	3·5	243	54
26,1	215	0·13	4370	24	0·006	0·000070	14	0·05728	1·0	0·416	1·1	0·05371	0·31	359·1	3·5	315	9·9
26,2	5·39	0·68	128	134	1·079	0·000374	53	0·04868	1·3	0·352	6·5	0·05790	2·80	306·4	3·9	304	150
27,1	199	0·12	4373	119	0·028	0·000068	20	0·05296	1·0	0·383	1·2	0·05348	0·44	332·7	3·3	306	14
27,2	32·2	0·72	819	371	0·468	0·000392	16	0·04547	1·0	0·329	2·3	0·05824	0·79	286·7	2·9	307	47
29,1	43·6	0·19	1038	525	0·522	0·000106	32	0·04878	1·0	0·351	1·6	0·05367	0·72	307·0	3·1	291	28
30,1	140	0·86	2673	109	0·042	0·000476	9	0·06057	1·0	0·453	2·3	0·06120	1·30	379·1	3·7	381	47

*Analysis not included in concordia diagrams and histograms in Fig. 11.
Errors are 1σ. Pb_c is common Pb. Error in standard calibration was 0·31% (not included in above errors but required when comparing data from different mounts). Common Pb corrected using measured ^{204}Pb in all isotopic ratios and ages.

with the maximum obtained for the samples of the intrusive units. Older ages of around 325–330 Ma (spots 27,1, 13,2 and 11,2, Table 2) and 350 Ma (spots 26,1 and 8,1, Table 2), coincide with the metamorphic peak and the start of the migmatization in the Spanish Central System, respectively (Montero *et al.*, 2004). A Devonian group of ages (370–410 Ma) is also present. These Devonian ages are older than the Variscan metamorphic peak and younger than the Ordovician ages determined in some regional metasediments and metavolcanic rocks (Valverde-Vaquero & Dunning, 2000; Bea *et al.*, 2007; Montero *et al.*, 2007). As discussed above, some of these Devonian ages are for analyses with low Th/U ratios, although this is not a general observation (spots 5,1 and 19,1), so that some confidence should be given to this age group. Similar ages have been previously described (e.g. Castiñeiras *et al.*, 2008), but they have been related to analytical error or mixed ages between thin rims and cores. The small number of eearly Cambrian ages (only spots 13,1 and 24,1) is noteworthy; these are dominant in other country rocks of the Central System batholith (Bea *et al.*, 2003; Zeck *et al.*, 2004; Castiñeiras *et al.*, 2008).

EXPERIMENTAL STUDY

Starting materials and procedures

Table 3 shows the compositions and mineral assemblages of the starting materials used in the experiments. The Bt

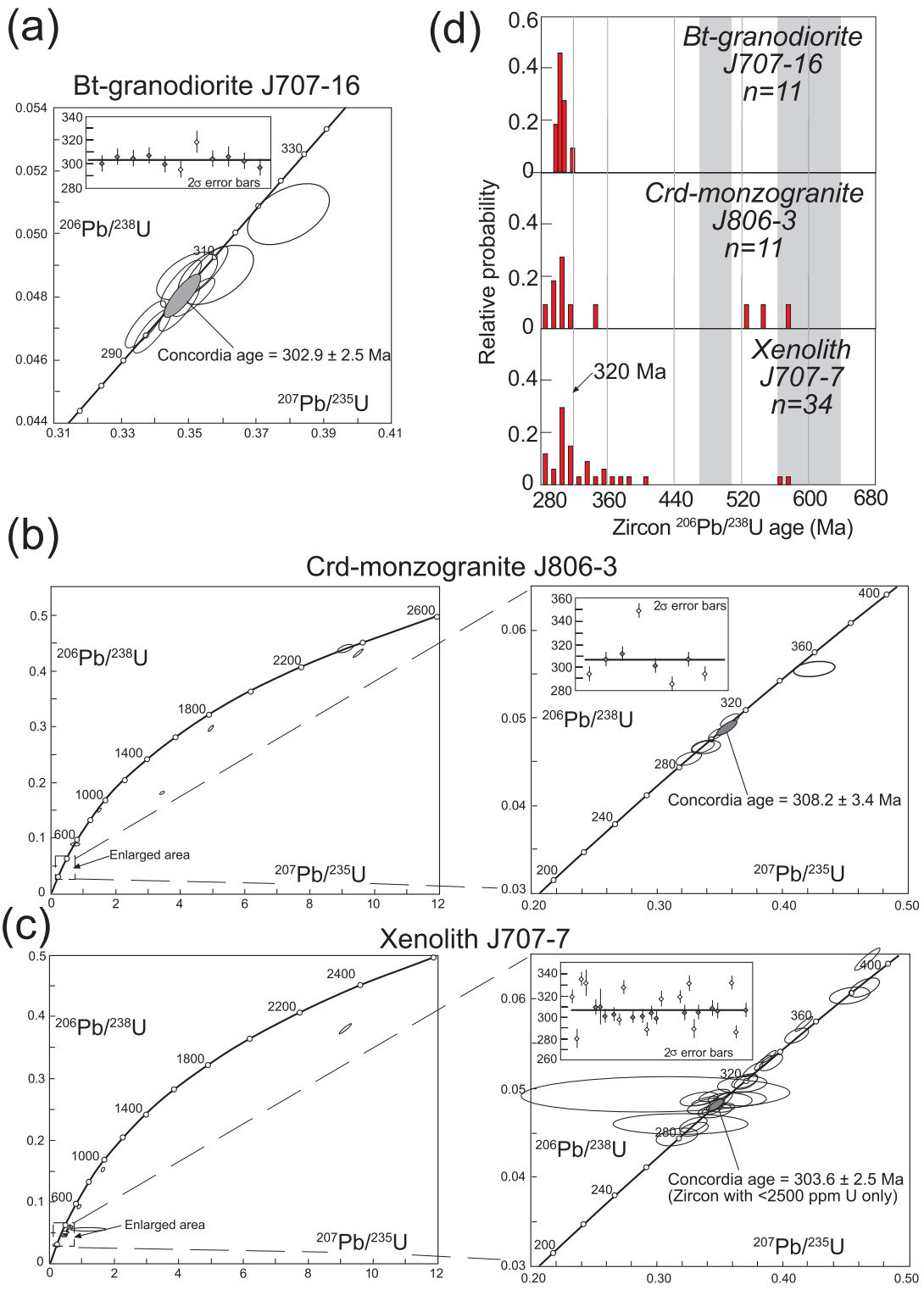

Fig. 9. U–Pb concordia diagrams and relative probability histograms for the three studied samples in Fig. 8. Data-point error ellipses in the concordia diagrams are 68·3% confidence limits, including the error from the standard, and include the 2σ error bars for ages between 280 and 350 Ma. Grey shaded ovoids are coherent groups of ages used to obtain the mean concordia age. (a) U–Pb concordia diagram for Bt granodiorite sample J707-16. (b) and (c) are concordia diagrams for the analyzed samples of Crd monzogranite (sample J806-3) and country rock xenolith (sample J707-7), respectively. An enlarged area plot for Variscan ages is also shown. (d) Relative probability histogram for the $^{206}Pb/^{238}U$ ages (listed in Table 2). Grey bands mark the main ages of the host sediments to the Central System batholith (see text).

Table 3: Chemical compositions and modal abundances (wt %) of the starting materials

Material	Ref.	SiO_2	TiO_2	Al_2O_3	FeO[1]	MgO	MnO	CaO	Na_2O	K_2O	P_2O_5	LOI	Total	Qtz[2]	Pl	Kfs	Bt	Ms	Crd
Bt-granodiorite[3]	J707-16	66·92	0·50	15·70	3·09	0·85	0·05	2·13	3·48	4·77	0·36	1·26	99·46	30	35	20	15	—	—
Xenolith (hornfels)[4]	J606-15	62·81	0·86	20·00	6·26	2·98	0·08	0·68	1·68	4·64	—	—	100·00	27	17	—	18	12	26
Cordierite[5]	—	49·54	—	33·27	8·06	8·62	0·30	0·02	0·05	0·17	—	—	100·08						

[1]Total iron as FeO.
[2]Mineral abbreviations after Kretz (1983).
[3]Bt-granodiorite from 'Puerto del Pico' 20 km from the contact with host rocks.
[4]Hornfels from the study area (see Fig. 1b).
[5]Fresh cordierite from 'El Pilón' cordieritites (Argentina, Rapela *et al.*, 2002).

granodiorite sample has the simple assemblage Bt, Qtz, Pl and Kfs, and was collected in an area several kilometres away from the contact (Puerto del Pico). The pelitic contaminant was taken from the large xenoliths of the Las Pozas outcrops (Figs 1b and 3a). Migmatitic hornfelses are characterized by a retrograde assemblage dominated by Chl, Bt, white mica, and Pl resulting from retrogression of Crd. The low-grade assemblage was preferred for the experimental simulation because water released by prograde reactions favours the attainment of equilibrium and simulates the natural effect of water supply from the thermal aureole into the intruding magma. Small fragments (50–100 μm) of this sample were mixed with the powder of the Bt granodiorite to simulate bulk assimilation. Part of the same sample was finely crushed and placed in single capsules. The phase assemblage and melt compositions from the pure end-members (i.e. the granodiorite and the xenolith) provide the baselines to make comparisons with the composite capsules that simulate magma–rock interaction. Fresh Crd crystals from the El Pilón cordieritites (Rapela *et al.*, 2002) and Sil-rich (>90 vol. % Sil) restitic nodules were used in experiments simulating selective assimilation of restitic residues. In all the composite capsules, 20 wt % of the contaminant was added to 80 wt % of granodiorite. A single layer or a mixed one with about 90 vol. % Crd crystals and 10 vol. % granodiorite powder was sandwiched between layers of pure granodiorite. With the exception of the run with the xenolith alone, water was added (4 wt % H_2O) with a microsyringe to the experiments. The textures of the Bt granodiorites and their comparison with predicted crystallization sequences in granite to granodiorite systems (Maaloe & Wyllie, 1975; Naney, 1983) indicate that the intrusive granodiorites were water undersaturated, possibly bracketed between the minimum represented by the water co-ordinated in hydrous minerals (*c.* 1 wt % H_2O) and the maximum representing saturation at the pressure of emplacement [*c.* 6 wt % H_2O according to the Burnham (1979) saturation model].

The experiments were performed at 850°C and 400 MPa. The absence of Grt and the conspicuous presence of Crd in the contact aureole of the batholith constrain the pressure of emplacement to a maximum of about 400–600 MPa. Field relations strongly indicate that assimilation of the country rocks took place at the level of emplacement, at the depth recorded by mineral assemblages in the contact aureole. Over large areas of the contact, the assimilated materials are migmatitic hornfelses developed locally around the contacts of the granodiorite sheets. The maximum pressure (*c.* 400 MPa) is recorded by the Crd ± Grt-bearing migmatites of the Peña Negra migmatites (Pereira & Bea, 1994) that overlie a granodiorite layer a few kilometres west of the Gredos area. Temperature was set at 850°C for all the experimental runs. This is the maximum value recorded by mineral assemblages with Crd ± Grt in the Peña Negra migmatites (Pereira & Bea, 1994), which were developed or re-equilibrated in the contact aureole of the intruding granodiorite. An independent criterion for choosing this temperature is based on the magmatic evolution of the intruding granodiorite. This is still rich in melt (>60 vol. % melt) at 850°C and may flow without viscosity limitations imposed by significant interactions between crystals. This is a minimum T for magma–rock interaction and assimilation. In the case of less evolved magmatic stages, the temperature can be higher and up to values close to 1000°C for low crystal contents (<10 vol. %) close to the liquidus. These values are based on the experimental results of this study (see below).

Experiments were conducted in a Boyd–England type piston-cylinder apparatus at the University of Huelva (Spain). A 12·5 mm (half inch) diameter cell was used in all the experiments. Details of the design of the cell have been given by Castro *et al.* (1999, 2010). Gold capsules (3 mm diameter and 0·15 mm thick) were filled, sealed by pressure folding and introduced into MgO pressure containers. Temperatures were measured and controlled with Pt100–Pt87Rh13 thermocouples wired to Eurotherm 808

controllers. Oil pressures were measured with electronic DRUCK PTX 1400 pressure transmitters, connected to OMRON E5CK controllers. Pressure was corrected manually and maintained within a narrow range of ±5 bar oil pressure, equivalent to ±250 bar on the sample. Heating proceeded at the maximum rate allowed by the system of 100 K min^{-1}. The hot-piston-out technique was used to minimize friction effects on the pressure container. To avoid relic phases in the run with the granodiorite end-member, temperature was set to 1050°C for 30 h and then lowered to the desired T of 850°C for 50 h. All minerals were re-equilibrated at the new conditions as demonstrated by the absence of zoning in Pl and the homogeneous composition of melt and minerals. After the desired run time, the experiments are quenched by switching the power off, which gives a cooling rate of more than 100 K s^{-1}. Fast cooling is crucial to avoid the formation of quench phases. After quenching, the capsules were examined for tears and checked for proximity of the thermocouple during the run. They were cut and polished for examination by electron microprobe. Experimental oxygen fugacity conditions are imposed by the assembly at conditions close to the quartz–fayalite–magnetite (QFM) buffer (Patiño Douce & Beard, 1996). Polished capsules were analyzed for major elements in mineral phases and glass (quenched melt) with the same electron probe microanalyser as used for the study of the natural rocks and using the same standards and ZAF corrections. A defocused beam 20 μm in diameter was used for glass analyses to minimize Na migration. In low melt fraction experiments, a smaller beam diameter was used to avoid contamination with X-rays from the surrounding phases.

Experimental results

Table 4 shows the phase assemblages, experimental conditions and compositions of melts and mineral phases for experimental runs with the end-members and the composite capsules. Representative back-scattered electron (BSE) images of the experimental capsules are shown in Fig. 10. Details of the textures and compositions are described below.

Granodiorite and xenolith end-members

The granodiorite-alone run contains about 62 vol. % melt (quenched glass) of leucogranite composition (Run 1, Table 4). This melt is rich in potassium ($K_2O = 4{\cdot}5$ wt %) and is peraluminous (ASI = 1·25). Plagioclase (29 vol. %) and Bt (7 vol. %) are the coexisting phases in equilibrium with the melt. The pelitic xenolith produced 37 vol. % melt of a potassium-rich and peraluminous leucogranite composition (Run 2, Table 4). This melt is poorer in Mg, Fe and Ca compared with the residual granite formed in the granodiorite run at the same P–T conditions. The potassium content is extremely high ($K_2O = 6{\cdot}5$ wt %), but comparable with that of many leucogranites from the same region formed by partial melting of similar pelitic sediments (Castro *et al.*, 1999, 2000). Euhedral Crd crystals (22 vol. %) were formed (Fig. 10a) together with new Kfs (12 vol. %), Bt (8 vol. %), Qtz (10 vol. %) and Pl (8 vol. %). Phase assemblages and compositions from these two experimental runs at 850°C and 400 MPa are used as a reference baseline to assess the changes produced in the melt by the interaction with the contaminants.

Crd-doped experiments

Cordierite in anatectic granites is a peritectic phase formed by incongruent breakdown of Bt in the presence of Qtz and Al-silicate. The implication is that Crd is formed together with melt in equilibrium. Both Crd and melt are reaction products and the granite magma is not necessarily saturated in the Crd components. Thus, the formation of Crd is not a simple process of magmatic crystallization when the magma is saturated in Crd. Our aim was to investigate the conditions for Crd stabilization in a system (granodiorite) in which we know *a priori* that Crd is not a stable phase but nevertheless exhibits textural relations (euhedral shape) that indicate equilibrium with the magma.

Selective assimilation of Crd crystals from the surrounding wall-rocks into the granodiorite has been simulated experimentally (400 MPa, 860°C; Runs 3 and 4, Table 4). The textural relations of phases and melt on both sides of the interface are shown in Fig. 10. It should be noted here that the Crd was not dissolved, but re-equilibrated to a more Mg-rich composition in a narrow band of a few micrometres thickness. The assemblage in the Crd-free layer consists of Pl(An_{53}) + Bt + Melt ± Ilm. This is similar to the assemblage in the run with the granodiorite alone. However, the melt experienced a slight increase in Al and K compared with the melt in the granodiorite-alone run. The assemblage inside the Crd layer consists of Crd + Bt + Pl(An_{51}) + Melt ± Ilm. Newly formed Crd crystals have the same Mg-rich composition as the external rims of the relic fragments of Crd (Fig. 10c and d). However, similar to the run with the Sil-rich spot, bulk equilibrium was not reached within the capsule. There is an effective, or reactive, system represented by the external rims of the Crd crystals together with Bt, Pl and melt. The run was repeated at a longer duration (150 h) than the original one (96 h). The results were almost identical in terms of phases and the absence of bulk equilibrium. The results described here correspond to the longer duration run. The only difference between the two runs is the presence of An-rich Pl (An_{90}) in the short duration run. In the longer run the Pl has a homogeneous composition. However, the melt in the Crd-rich layer of the capsule is poorer in Ca compared with the melt in the Crd-free layer. With the exception of the Ca content the melt is homogeneous across the two layers. The observed mineral assemblages are compatible with at

Table 4: Experimental conditions and phase compositions

Starting material	Added contam.	*P* (GPa)	*T* (°C)	Duration (h)	Water (wt %)	Assemblage	Phase	SiO_2	TiO_2	Al_2O_3	FeO_t	MgO	MnO	CaO	Na_2O	K_2O	P_2O_5	Total	100 – total	ASI	Mg-no.	An%
Run 1, GS_34																						
J707-16		0·4	860	50	4	Gl (62), Pl (29), Bt (7),	Gl	76·99	0·31	13·52	0·91	0·31	0·01	1·44	2·09	4·40	0·01	100	10·05	1·25	38	24
(Bt-gran.)						Mgt (<2)	Pl	57·95	—	24·94	0·96	—	—	9·45	5·17	0·54	—	98·60				66
							Bt	39·19	4·94	14·15	10·16	17·46	—	—	0·91	8·56	—	95·18			75	
Run 2, EA-11																						
J606-15		0·4	850	120	0	Gl (37), Crd (22),	Gl	75·95	0·31	13·55	0·84	0·15	0·06	0·44	2·17	6·45	0·10	100	3·63	1·19	24	7
(xenolith)						Kfs (12), Qtz (10),	Crd	43·61	0·13	38·04	9·24	7·05	0·23	0·26	0·29	0·94	0·02	99·93			58	
						Bt (8), Pl (8), Spl (<2)	Pl 1	62·85	0·08	23·97	0·19	0·02	0·01	4·54	8·34	0·22	0·14	100·43				37
							Pl 2	60·47	0·02	24·69	0·33	0·03	0·03	7·04	5·00	1·74	—	99·70				56
							Bt	36·77	2·99	21·31	18·85	8·41	0·14	0·01	0·38	9·39	0·04	98·90			44	
							Spl	8·45	0·37	44·66	40·40	5·16	0·34	0·10	0·11	0·75	—	100·49			19	
							Kfs core	56·12	0·15	28·61	0·27	0·03	—	1·66	2·68	9·04	0·04	99·58				
							Kfs rim	63·65	0·08	19·31	0·19	0·01	—	0·26	2·17	12·29	0·24	99·44				
Run 3, EA-5																						
J707-16	Crd	0·4	850	150	4	Mixed zone	Gl	72·04	0·04	17·77	1·77	0·49	0·12	1·01	2·89	3·36	0·51	100	7·84	1·74	33	18
	(20 wt %)					Gl (17), Crd core (44),	Crd core	47·86	—	33·10	7·75	8·46	0·27	0·04	0·19	0·05	—	97·83			66	
						Crd rim (<3), Bt (7),	Crd rim	48·06	0·05	33·31	4·71	10·66	0·12	0·10	0·38	0·11	0·01	97·51			80	
						Pl (28)	Bt core	35·51	5·42	17·16	16·51	11·62	0·14	0·03	0·86	8·57	—	96·97			56	
							Bt rim	37·79	0·67	18·05	13·34	16·36	0·12	0·02	0·73	7·86	—	95·26			69	
							Pl	59·14	0·02	25·12	0·26	0·02	—	6·83	6·87	0·58	—	99·11				51
						Crd-free zone	Gl	72·60	0·09	17·05	1·55	0·36	0·09	1·36	2·94	3·58	0·38	100	8·53	1·53	29	22
						Gl (78), Pl (15), Bt (5),	Bt	35·29	4·07	17·64	15·52	12·64	0·11	0·03	0·88	8·41	0·02	95·11			59	
						Ilm (<2)	Pl	59·12	0·02	25·43	0·16	0·02	—	7·26	6·76	0·49	—	99·26				53
Run 4, EA-7																						
J707-16	Crd	0·4	850	96	4	Mixed zone	Gl	75·11	0·40	14·67	0·83	0·20	0·06	0·82	2·50	5·22	0·19	100	4·94	1·30	30	13
	(20 wt %)					Gl (16), Crd core (55),	Crd core	48·12	—	33·76	7·67	8·62	0·24	0·03	0·05	0·08	0·02	98·58			67	
						Crd rim (15), Pl (10),	Crd rim	48·46	0·01	34·46	5·69	10·08	0·29	0·06	0·05	0·05	0·02	99·21			76	
						Ilm (4)	Pl	58·68	0·06	25·30	0·49	0·05	0·01	6·45	6·44	1·20	0·25	99·13				50
						Crd-free zone	Gl	73·98	0·38	15·49	0·72	0·46	0·06	1·10	2·50	4·97	0·34	100	5·08	1·35	53	17
						Gl (68), Pl (25), Bt (5),	Pl core	51·29	0·06	30·22	0·55	0·03	0·03	12·62	3·54	0·40	0·12	98·90				79
						Ilm (<2)	Pl rim	57·07	0·08	26·65	0·32	0·03	0·04	8·43	5·66	0·63	0·05	99·02				61
							Bt	35·29	4·07	17·64	15·52	12·64	0·11	0·03	0·88	8·41	—	95·11			59	

(continued)

Table 4: Continued

Starting material	Added contam.	*P* (GPa)	*T* (°C)	Duration (h)	Water (wt %)	Assemblage	Phase	SiO_2	TiO_2	Al_2O_3	FeO_t	MgO	MnO	CaO	Na_2O	K_2O	P_2O_5	Total	100 – total	ASI	Mg-no.	An%
Run 5, EA-8 Sil																						
J707-16	Sil (20 wt %)	0·4	850	240	4	Mixed zone	Gl	75·75	0·23	14·42	0·52	0·33	0·06	0·40	2·31	5·86	0·13	100	4·45	1·33	53	7
						Gl (9), Sil (82), Pl (6),	Crd	49·56	0·05	34·52	1·47	12·67	0·17	0·08	0·16	0·32	0·02	99·05			94	
						Crd (<2), Ilm (<1)	Pl	56·92	—	27·61	0·25	0·05	0·01	7·37	5·83	1·08	0·03	99·40				55
						Sil-free zone	Gl	76·69	0·22	13·70	0·56	0·33	0·05	0·38	2·21	5·75	0·12	100	4·58	1·30	51	7
						Gl (56), Pl (24),	Pl core	48·86	0·01	32·38	0·41	0·09	0·07	13·74	2·82	0·42	0·20	99·08				83
						Qtz (8), Bt (6), Kfs (3),	Pl rim	56·92	—	27·61	0·25	0·05	0·01	7·37	5·83	1·08	0·03	99·40				55
						Ilm (<2), Ap (<1)	Bt	41·70	3·84	17·01	9·37	15·67	0·09	0·10	0·50	8·57	0·01	97·05			75	
							Kfs	64·22	0·04	19·05	0·06	0·01	—	0·05	2·41	13·23	0·02	99·18				
Run 6, EA-8 Xen																						
J707-16	Xen (20 wt %)	0·4	850	240	4	Gl (59), Pl (13), Qtz (7),	Mixed zone															
						Bt (7), Kfs (5), Crd (4),																
						Sil (2), Spl (2), Ilm (<1),	Gl	74·48	0·21	15·06	0·90	0·27	0·04	0·52	2·37	6·06	0·09	100	4·88	1·32	35	8
						Ap (<1)	Crd	48·02	0·01	34·11	9·49	7·40	0·40	0·04	0·10	0·22	—	99·81			58	
							Bt	34·48	2·94	21·04	18·28	8·96	0·14	0·04	0·42	9·36	0·03	95·86			47	
							Spl	0·89	0·27	53·64	31·68	12·77	0·49	0·02	0·03	0·09	—	99·91			42	
							Kfs	64·37	0·02	18·75	0·12	0·02	—	0·12	2·42	13·01	0·07	99·08				
							Xen-free zone															
							Gl	76·81	0·19	13·58	0·62	0·28	0·03	0·41	2·13	5·86	0·09	100	4·99	1·28	44	7
							Pl core	62·58	—	23·20	0·13	—	—	3·86	9·03	0·24	0·02	99·13				32
							Pl rim	58·20	0·06	25·79	0·29	0·02	—	7·10	6·31	1·45	0·02	99·48				52
							Bt	41·70	3·84	17·01	9·37	15·67	0·09	0·10	0·50	8·57	0·01	97·05			75	
							Kfs	64·37	0·02	18·75	0·12	0·02	—	0·12	2·42	13·01	0·07	99·08				

Average values in wt % oxides for a total numbers of analyses from four to 10 points. Standard deviations (1σ) are 1·06–0·22 for SiO_2, 0·05–0·02 for TiO_2, 0·73–0·19 for Al_2O_3, 0·08–0·02 for FeO, 0·08–0·01 for MgO, 0·18 (only EA-5 and EA-7) to 0·05 for CaO, 0·24–0·04 for Na_2O, 0·38–0·04 for K_2O, 0·01 for P_2O_5 and 0·87–0·33 for 100 – total. Added contam., added contaminant; Bt-gran., Bt-granodiorite. —, abundances below the detection limit. Numbers in parentheses beside phases and glass are modal abundances (wt %) measured by image analysis. Mineral abbreviations are after Kretz (1983); Gl, glass.

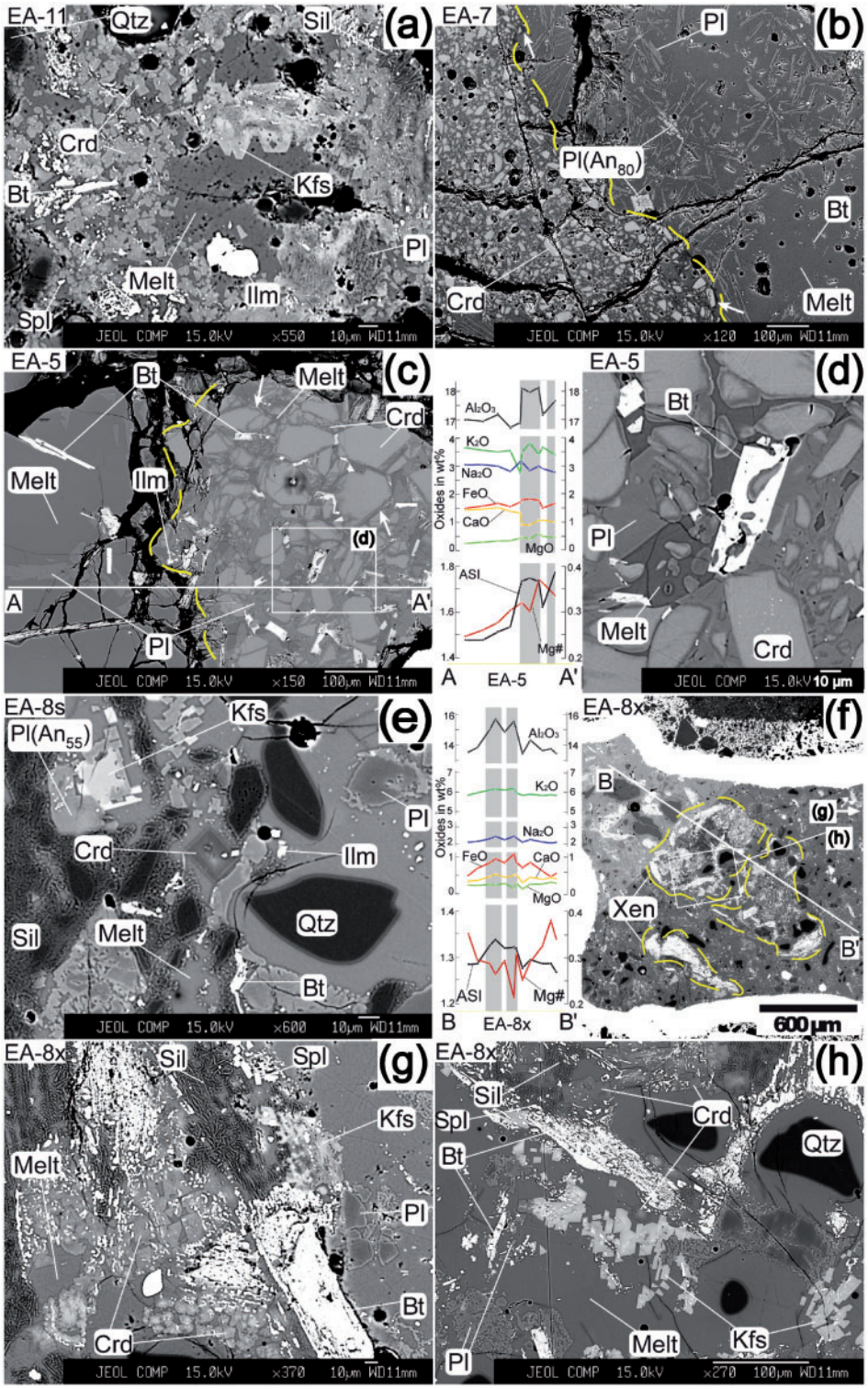

Fig. 10. BSE images of experimental runs simulating the interaction between Bt granodiorite and potential mineral and rock contaminants. All experiments were carried out at 850°C and 400 MPa. (a) Pelitic xenolith end-member. (b), (c) and (d) show the textures of runs with addition of Crd to the Bt granodiorite. (e) Texture and mineral assemblage of the run with addition of a Sil-rich spot to the Bt granodiorite. (f), (g) and (h) show the textures and mineral phases in the experiment with addition of a fragment of pelitic xenolith to the granodiorite. Compositional profiles of the melt across the capsules are shown in (d) and (f). (See text.)

least two effective subsystems (Fig. 11a). The position of these subsystems is far from the Crd end-member even when Crd is the most abundant mineral.

Sillimanite-doped experiments

A small fragment of a Sil-rich spot (Sil > 90 vol. %) was added (20 wt %) to the Bt granodiorite powder in composite gold capsules (Run 5, Table 4). At the interface with the Sil spot, euhedral Crd crystals were formed (Fig. 10e). The new assemblage in the area close to the Sil spot consists of Sil, Bt, Pl, Kfs, Crd, Ilm and Qtz. The cores of newly formed Pl near the Sil spot are rich in An ($An_{83}Ab_{14}Or_3$), whereas their rims are compositionally equilibrated ($An_{55}Ab_{40}Or_5$) to the P–T conditions of the experiment (0·4 GPa, 850°C). The melt (57 vol. %) changed in composition with respect to the residual liquid of the Bt granodiorite at the same P–T conditions (Table 4). The new melt is poorer in Fe, Mg and Ca and richer in K. Most of the Ca in the system is captured by the An-rich Pl formed in the vicinity of the Sil-rich spot. Apart from this local situation, we observed several incompatible assemblages that may indicate at least four subsystems in the bulk capsule (Fig. 11b).

Pelite-doped experiment: bulk assimilation

Reactive bulk assimilation, as defined by Beard *et al.* (2005), was experimentally simulated by addition of a small fragment (xenolith) of a fine-grained metapelite to the granodiorite magma (Run 6, Table 4). After a long duration of 10 days (240 h), the boundaries of the fragment were still recognizable in the capsule (Fig. 10f). Subtle differences in the compositions of melt across the xenolith and between the minerals were observed. The assemblage within the area occupied by the metapelite fragment is Crd + Sil + Bt + Spl + Qtz + Kfs + Melt. In the area surrounding the fragment the assemblage is Pl + Qtz + Kfs + Bt + Melt. The large number of phases indicates that the system is far from equilibrium. However, the euhedral habit and homogeneous composition of Crd in the area surrounding the xenolith, together with the homogeneous composition of the melt, strongly suggest that at least these two phases, melt and Crd, are in chemical equilibrium in the capsule. The melt has a peraluminous leucogranite composition with low contents of Fe, Mg and Ca, and an ASI value of 1·2 (Table 4). The only appreciable difference is a higher content in Al ($Al_2O_3 = 15{\cdot}06$) within the area of the xenolith compared with a lower value ($Al_2O_3 = 13{\cdot}58$) in the area outside the xenolith. These differences in Al are related to the high Al content of the xenolith, in which Sil and Spl coexist with Crd and melt. It is noteworthy that these differences have survived for 240 h in a water-bearing system and at a scale of several micrometres. Although the composition of the melt is peraluminous and constant across the capsule, Crd forms only in the xenolith area, where the peritectic reaction took place. Biotite compositions record these slight differences in Al activity between the two areas. The tschermakitic component of Bt increases in the xenolith area compared with the area of the granodiorite magma. These changes in phase composition are depicted in an ACF diagram (Fig. 11c). Although bulk equilibrium is not completely reached, the two subsystems (i.e. xenolith and magma) tend to converge as indicated by the shift in the compositions of the melt and the Bt with respect to the compositions in the experiments with the respective end-members. The most important change in the composition of the melt in the granodiorite area is a significant increase in K ($K_2O = 5{\cdot}86$ wt %) compared with the composition of the melt in the granodiorite-alone run ($K_2O = 4{\cdot}40$ wt %). This phenomenon occurs in parallel with the appearance of new-formed, euhedral Kfs in the composite charge. This phase was absent in the granodiorite-alone experiment.

DISCUSSION

Indicators of reactive bulk assimilation

Several lines of evidence clearly support the working hypothesis that Crd monzogranites are the product of interaction between an intruding Bt granodiorite magma and pelitic country rocks. Clear indicators of assimilation come from: (1) field relations at scales from outcrop to pluton; (2) geochemical variations in major elements; (3) the data provided by the inherited zircons in the studied samples; (4) the determination of phase relations by means of laboratory experiments.

Implications from field relations

Field relations show that there is a clear correlation between the presence of Crd in the granitoids and the proximity to the contact with the country rocks. The same general observation in neighbouring areas of the Central System batholith was previously interpreted as resulting from country rock assimilation (Ugidos *et al.*, 2008). However, interesting details about the mechanism and the feasibility of the assimilation process remained unexplained. Our detailed mapping of the Crd-bearing granitoids in the Gredos area (Fig. 1) shows not only that Crd is preferentially concentrated near the contact with the country rocks, but also that the concentration of Kfs is positively correlated with the abundance of prismatic Crd in the granitoids (Fig. 4), which are monzogranites and not granodiorites when they contain Crd. The simple view that Crd is a xenocrystic phase is not sufficient to account for the observed field relations. Both phases, Crd and Kfs, typically have a euhedral habit, strongly suggesting crystallization from a melt. This observation contradicts our previous experimental results (García-Moreno *et al.*, 2006), which strongly suggested that Crd is not in equilibrium in a magmatic system with the composition of the whole-rock (monzogranite) in which it appears.

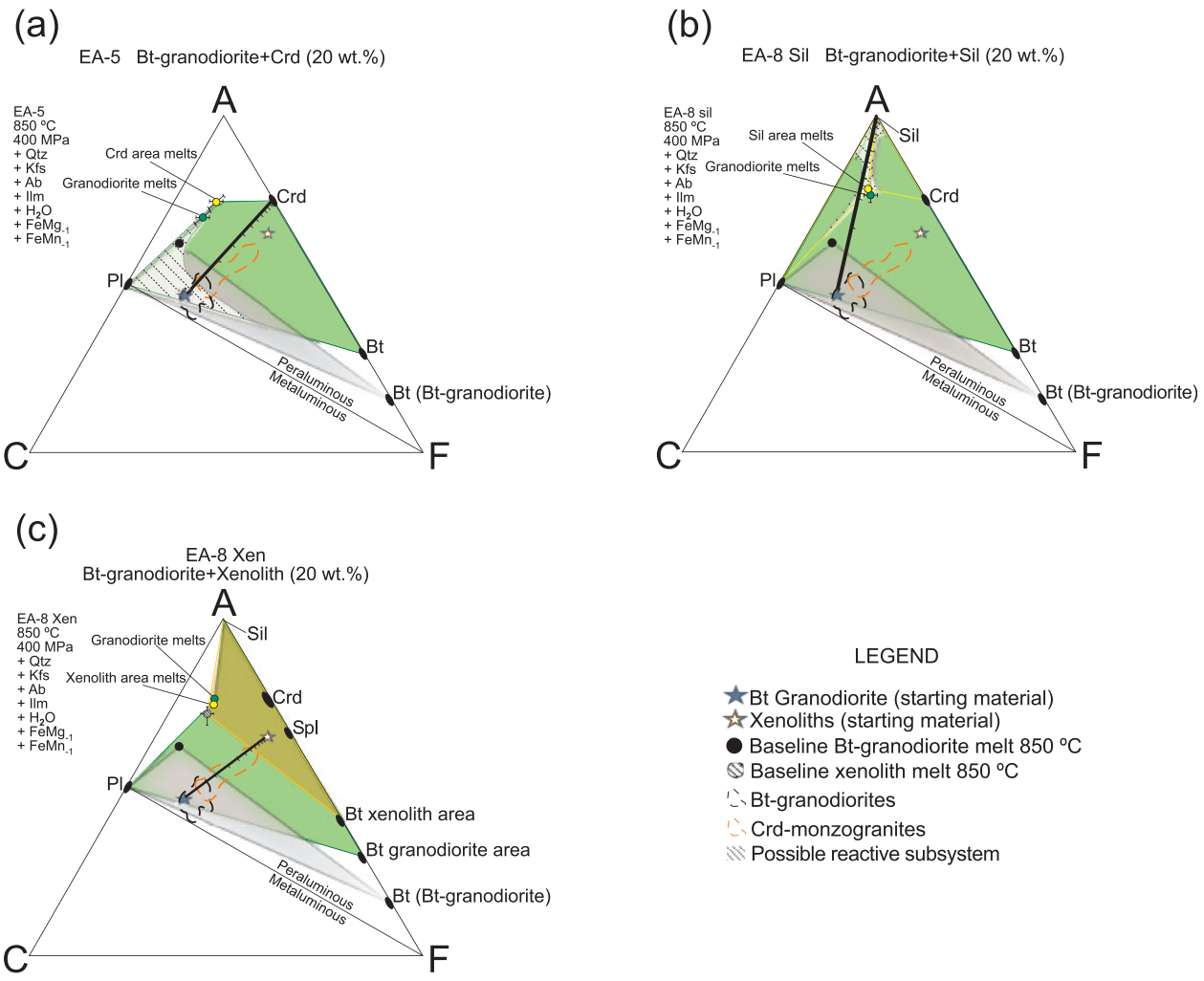

Fig. 11. ACF projections (A = Al_2O_3; C = CaO; F = FeO) showing the coexisting mineral assemblages and melts in the composite experimental runs with the addition of Crd (a), Sil-rich spot (b), and xenolith (c) to the Bt granodiorite. Molar proportions of ACF are projected by algebraic inversion of the compositional space defined by the components A, C, F, Qtz, Kfs, Ab, Ilm, H_2O and the exchange vectors $FeMg_{-1}$ and $FeMn_{-1}$. The area of the reactive subsystems has been traced tentatively according to qualitative observations of textures in the runs. The bold line with tick marks is the bulk mixing line of the two systems represented by the Bt granodiorite and the contaminant. Tick marks represent 10 wt % proportions of one of the two end-members. The composition of the Crd monzogranites is close to the mixing array using the xenoliths as contaminants (c). (d) represents the constant slope of the Mg-number partitioning between Crd and Bt supporting the shift in composition of the local system with time. It should be noted that newly formed Bt, both in the granodiorite layer and the Crd-rich layer, is richer in Al with respect to the baseline represented by the Bt composition in the granodiorite alone. The four-phase assemblage depicted in (a) and (c) indicates the peritectic reaction that forms Crd at the expense of Bt. The remaining melt in the granodiorite system alone at the same P–T conditions is very close in aluminosity to the melts formed in the composite capsules. These relations point to potential equilibrium of Crd in the residual melt of a partially crystallized granodiorite.

The heterogeneous distribution, which is not typical of magmatic minerals in plutonic rocks, also conflicts with the euhedral shape. Field relations show that the granodiorite intruded forming tabular bodies with a maximum thickness of about 1000 m and extending laterally for several kilometres. Assimilation is favoured when the intrusive granodiorite is in contact with low-grade metasediments. Textural features within metasedimentary xenoliths, along with the magma–magma contacts observed between granitoids and leucocratic veins, indicate that they were heated and metamorphosed during their inclusion in the host magma body. Indeed, these metasediments retain the appearance of typical fine-grained hornfelses. The process seems to be less effective if the granodiorite intrudes into migmatites. These observations point to a greater effectiveness of the assimilation process when the country rocks were previously unmetamorphosed at high grade. Most hydrous

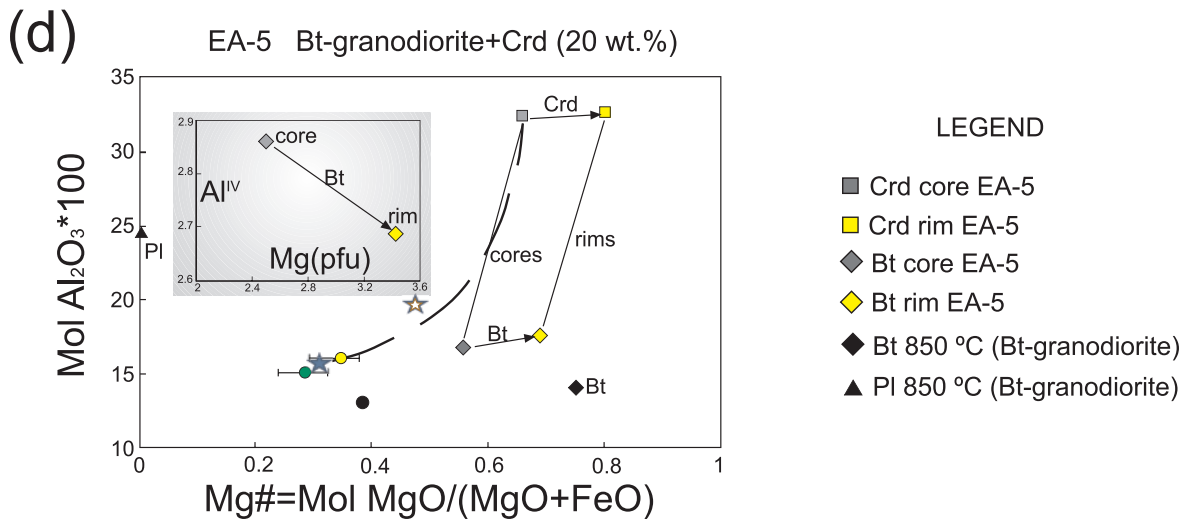

Fig. 11. Continued.

minerals (e.g. chlorite) were still present in the pelitic wall-rocks at the time of granodiorite emplacement. Water released within the thermal aureole probably triggered thermal shock and dismemberment of the migmatitic hornfelses into small, centimetre- to metre-sized blocks that were enclosed by the intruding magma.

Inherited zircons

The presence of inherited zircons in granitic rocks is commonly interpreted in terms of local assimilation of country rocks (Beard *et al.*, 2005; Clarke, 2007). In the case of anatectic granites, derived from polygenetic metasedimentary sources (pelites and greywackes), the inherited zircon may be incorporated as inclusions in restitic minerals or as isolated crystals. In our case this interpretation is based on two main observations, as follows. (1) Inherited zircon cores have not been observed in samples of granodiorites collected several kilometres away from the area of contamination and assimilation of the country rocks. (2) Inherited cores observed in the contaminated granites have the same morphology and ages (548–575 Ma; Fig. 8) as those found in the country rocks in this region. Other ages in relic cores are 10–40 Myr older than the age of the magmatic rims that represent the time of magma emplacement and crystallization. These ages may represent the early stages of Variscan migmatization reported by Montero *et al.* (2004).

The meaning of geochemical variations

The geochemical characteristics of the granitoids are also in agreement with a process of bulk assimilation. The observed variations in major and trace elements provide strong evidence that this process was responsible for the generation of the Crd monzogranites (ACU). Departures from cotectic-like evolution of the liquid compositions are among the most compelling observations. For example, in the CaO–MgO diagram (Fig. 6d), in which fractional crystallization is well defined by a regular trend of covariation, the Crd monzogranites plot along forbidden lines for magmatic evolution with increasing MgO and decreasing CaO in the residual liquid. Interestingly, the Crd monzogranites plot along trends that link a particular point on the cotectic-like trend (e.g. in the CaO–MgO diagram) with the average composition of the country rock metapelites. These transverse trends are completely unrelated to any change in pressure or water content. The intersection of this trend with the cotectic marks the composition of the magma at the time of assimilation of the country rocks. It is important to emphasize here that the Bt granodiorite magma that arrived at the level of emplacement, where wall-rock assimilation occurred, was already highly differentiated. Some granodiorites plot along the cotectic line above the intersection point (Fig. 6d). In this evolved region of the diagram, close to the ternary minimum, the cotectic lines for water-undersaturated systems tend to converge toward the minimum melt composition. Thus, it is difficult to know if the more evolved members of the Bt granodiorite that trend down from the assimilation intersection point are low-pressure fractionates produced at the level of emplacement or fractionated pulses of magma coming from depth.

These compositional relations not only tell us about the composition of the assimilating magma, which we need to estimate the amount of assimilated material by mass balance, but they also are definitive in distinguishing selective from bulk assimilation. The assimilation trends point to the composition of the country rocks (i.e. metapelites), not to a particular mineral composition. This position is

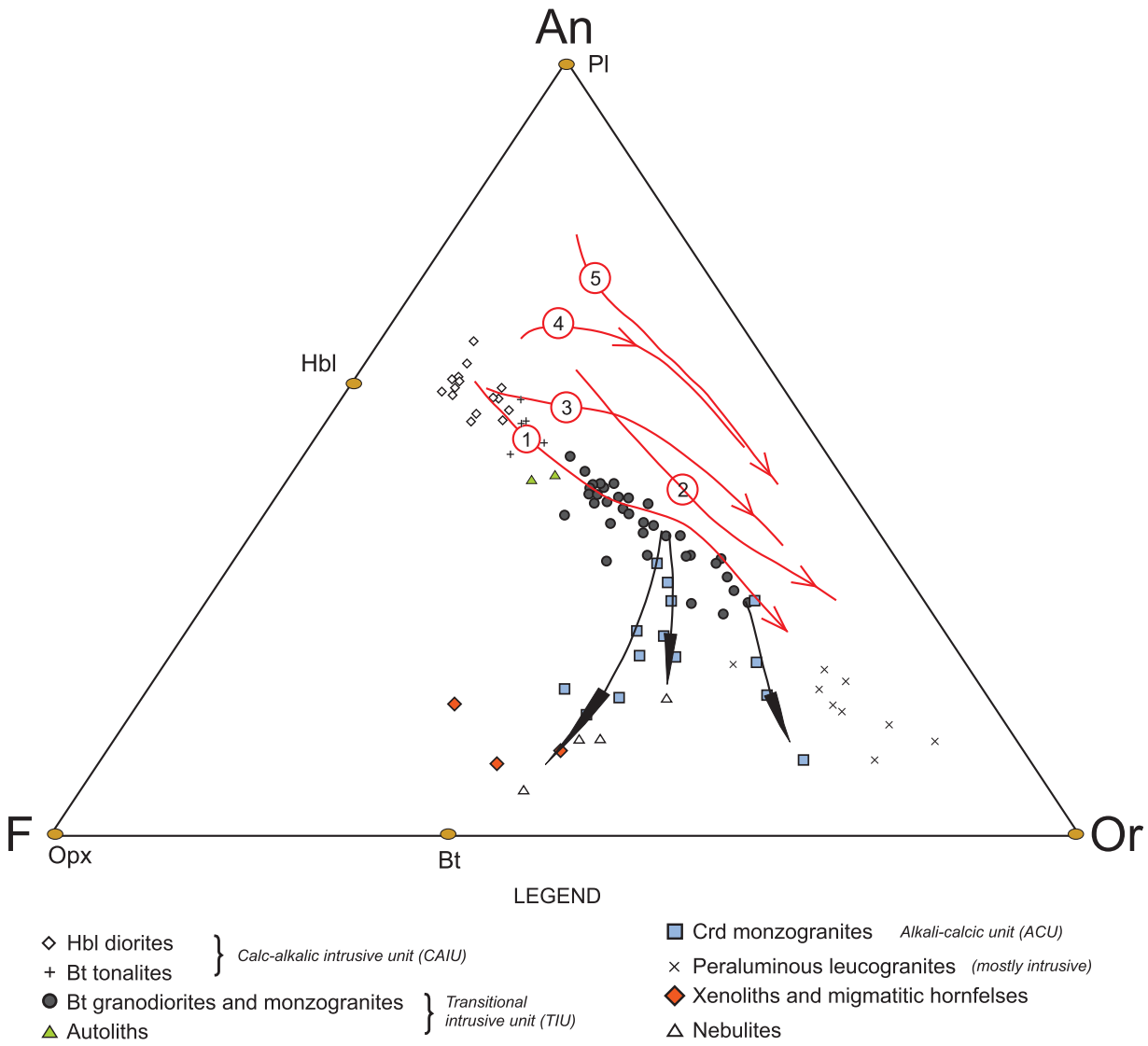

Fig. 12. Projection of the granitoids of the Gredos massif into the pseudoternary system defined by Opx–Or–An. Lines of multi-saturation (cotectic-like) are traced from experimental data in calc-alkaline systems. These represent liquid trajectories by either crystal fractionation or partial melting. Arrows mark the direction of decreasing *T*. The Bt granodiorites of Gredos follow the cotectic trend, corresponding to liquids produced either by fractionation of an andesitic parental magma or by partial melting of a diorite source. The Crd monzogranites follow a trend transverse to the general trend of the cotectic lines. The main transverse trend points to the composition of the country rock pelitic xenoliths. These relations suggest that the Crd monzogranites result from bulk assimilation of pelitic metasediments by a Bt granodiorite magma. Cotectic lines (1) and (3) correspond to experiments by Sisson *et al.* (2005) at $P = 700$ MPa and 2·3 and 1·7 wt % H_2O respectively; (2) Castro *et al.* (2010) at $P = 1{\cdot}5$ GPa and 0·9 wt % H_2O; (4) Carroll & Wyllie (1990) at $P = 1{\cdot}5$ GPa and 2·5 wt % H_2O; (5) Skjerlie & Patiño Douce (2002) at $P = 2{\cdot}1$ GPa and <2 wt % H_2O.

intermediate between Bt and Or and closer to Bt (Fig. 12). According to these relations, the Crd monzogranites are variably enriched in Fe, Mg and K with respect to the intruding granodiorite magma. This observation is in agreement with the observed correlation between the increase in the amount of Crd and Kfs megacrysts in the granitoids close to the contact with the pelite host (Fig. 4a and b). The conclusion is that bulk, and not selective, assimilation is the process responsible for the observed relationships.

The assimilation trends defined by the Crd monzogranites are, therefore, out of any cotectic or any other equilibrium relationship in the F–Or–An diagram (Fig. 12). The meaning of this is that the Crd monzogranites do not represent a magmatic system in which Crd and melt coexist in equilibrium. A possible explanation is that Crd formed

in the course of a peritectic reaction in country rock xenoliths at the time of xenolith disaggregation and dispersion of other components in the magma as proposed for reactive bulk assimilation (Beard *et al.*, 2005). In this case, the Crd may have survived resorption by the magma as the newly formed crystals are in local equilibrium with a local melt (the reactive magma; Pichavant *et al.*, 2007)

Geochemical variations for REE (Fig. 7) are also in agreement with contamination. The Crd monzogranites display REE patterns similar to those of the non-contaminated Bt granodiorites. The REE patterns of the two main contaminants in the study region (i.e. hornfelses and Crd-rich nebulites) are similar each other (Fig. 7d). They show strong HREE depletion and their effect as a contaminant is to produce a slight depletion in the Crd monzogranites compared with the intrusive Bt granodiorites.

Constraints provided by the laboratory experiments

Our experimental investigation of selective assimilation of Crd xenocrysts shows that Crd can be a stable phase in local subsystems of the granodiorite magma (Runs 3 and 4, Table 4). Although selective incorporation of Crd from the wall-rocks seems unlikely in the study area based on the analysis of geochemical variations, our experiments shed light on how Crd crystals can survive within a Bt granodiorite magma. Melt in the Crd-free and Crd-rich layers, as well as in the granodiorite-alone run at the same P–T conditions, has the composition of a peraluminous leucogranite, and is almost identical to experimental melts (Patiño Douce & Johnston, 1991; Castro *et al.*, 2000) formed in equilibrium with Crd by Bt breakdown in pelitic metasediments. These melts are also compositionally similar to Crd-bearing anatectic leucogranites in the Gredos area. In all these cases, melts and natural rocks, Crd is in equilibrium with a moderately peraluminous melt (ASI = 1·2–1·4). With the exception of local equilibrium at the Crd–melt boundary layer, which may produce a local increase in Al activity over a small area, our results indicate that Al solubility, recorded by the ASI or the amount of normative corundum, is not strongly dependent on the presence of an Al-rich mineral in equilibrium with the melt. Experiments in the haplogranite system have shown (Acosta-Vigil *et al.*, 2003) that Al solubility is strongly dependent on the amount of dissolved water in the melt and, to a minor extent, on the presence of non-haplogranitic components, specifically Fe, Mg and Ca. Our melt compositions are not pure haplogranitic, although they are peraluminous leucogranites with low contents of Fe, Mg and Ca. Because water diffuses several orders of magnitude faster than cations in silicate melts, the water content of both anatectic melts in the migmatite xenoliths and residual liquids from granodiorite crystallization can be close in composition to each other and, consequently, the Al solubility can be also similar. The existence of a boundary local equilibrium in the Crd-doped experiments, which was formed at the beginning of reaction between the added Crd and the granodioritic melt, is supported by the reverse compositional zoning (Mg-number is higher at the rim) of newly formed Bt (Fig. 11d). The composition of the local melt around the Fe-rich Crd crystals was possibly richer in Al and Fe, in local equilibrium with the dissolving Crd. Thus, Ca was possibly trapped by An-rich Pl in the Crd-rich layer of our composite capsules and not released to the melt during re-equilibration of the whole system. It must be noted that local equilibria of this kind are not exclusive to experimental capsules; they may be found at variable scales in nature (Pichavant *et al.*, 2007). In summary, the experiments on the Bt granodiorite-alone show that these magmas cannot precipitate Crd. However, added Crd can survive in equilibrium with the peraluminous residual melts of the Bt granodiorite. These phase relations are fundamental to understanding the presence of euhedral Crd in the monzogranites resulting from the assimilation process.

Selective addition of an Al-silicate phase (e.g. Sil, Run 5, Table 4) was also tested in our experiments. The presence of Sil-rich restitic spots is a general feature of the nebulitic migmatites that host the intrusive granodiorite sheets in the Gredos area. Our experiments show that Crd may be formed in local domains in proximity to the Sil-rich spots. The euhedral habit of Kfs, together with the appearance of euhedral Crd (Fig. 10e), suggests the existence of a reaction of the type

$$\begin{aligned}\text{granodiorite (bulk)} + \text{xenolith (Sil-rich)} \rightarrow \\ \text{Crd} + \text{Pl}\ (\text{An}_{55}),\ \text{Pl}\ (\text{An}_{>90}) + \text{Bt} + \text{Ilm} \\ + \text{Qtz} + \text{Kfs} + \text{Melt}.\end{aligned} \qquad (2)$$

This is not a balanced reaction. It is inferred from textural observations and modal changes in the new coexisting assemblage. Reaction with the bulk granodiorite system is unlikely because it is partially crystallized at the conditions of the experiments. Thus, only the residual melt (granitic) is available to react with the Sil-rich contaminant. However, it is expected that the new phases formed in the granodiorite magma tend to be in equilibrium with the new contaminated system. Although equilibrium is not reached in the capsule, the observed assemblages provide useful information about the way the system changes as a response to changing composition. A new local assemblage consists of Pl (An_{55}) + Bt + An-rich Pl + Ilm. This is in local equilibrium with a new melt that departs considerably from the residual melt of the granodiorite system in the absence of the contaminant at the same P–T conditions (Run 1, Table 4).

These local domains near the Sil-rich spot represent local equilibrium in the boundary layer surrounding the dissolving crystals (e.g. Kuo & Kirkpatrick, 1985; Tsuchiyama, 1985). The formation of An-rich Pl is evidence

of these local boundary layer melts in which the extremely high Al activity provokes the formation of An, which is preserved as a metastable phase, surviving re-equilibration because of the slow diffusion rate (D) for the $NaSiCa^{-1}Al^{-1}$ interchange in Pl ($D \sim 10^{-20}\,cm^2\,s^{-1}$; Grove *et al.*, 1984).

Our experimental results demonstrate that reaction between pelitic xenoliths and the granodiorite magma does not impede the generation of Crd, formed in equilibrium with the melt in a local domain—the disintegrating xenolith—where the reactants to the peritectic reaction are located. The formation of Kfs, together with Crd in these domains, supports this interpretation. Interestingly, the composition of the melt outside the xenolith area is close in composition to that of the melt inside the xenolith area where Crd and melt are in contact. These melts are in turn similar to the composition of the residual melt at 850°C and 400 MPa in the experiment with the granodiorite alone. The fact that the residual melt of the granodiorite magma is a peraluminous leucogranite makes it possible to retain Crd crystals, which are formed inside the entrapped xenoliths, in equilibrium with the effective subsystem of the granodiorite magma (i.e. the subsystem represented by the residual melt). Our experiments also show that K released from the xenolith fluxed this residual melt. Because K is a mobile element in silicate melts, its concentration is homogenized throughout the capsule, inducing the crystallization of Kfs. We have shown that the appearance of Crd in the contaminated granites is accompanied by the formation of Kfs megacrysts (Fig. 4). The bulk-rock composition of the intruding granodiorite is shifted to monzogranitic in areas where they are rich in Crd. According to the phase equilibria shown by our experiments, the formation of the large Kfs megacrysts that characterize the studied monzogranites is induced by an increase in the K content of the magma resulting from assimilation of pelitic xenoliths. This K increase may happen at any stage of the crystallization sequence, depending on the melt content of the intruding magma at the time of its emplacement and subsequent wall-rock assimilation. In the field, the presence of flow structures that orientate the Kfs megacrysts (Fig. 3b) indicate that they were formed in a low-crystallinity system, which was still able to flow. This observation is compatible with our experimental results predicting a melt content of about 60 vol. % at the time of magma interaction at 850°C and 400 MPa, well above the critical melt fraction for the dramatic strength drop of partially melted silicate materials (e.g. van der Molen & Paterson, 1979; Lejeune & Richet, 1995) and, therefore, within the flow field of a liquid-supported aggregate. At this degree of crystallinity, the composition of the residual melt is close to that of a peraluminous leucogranite and may act as a reactive subsystem that maintains Crd formed in trapped xenoliths in equilibrium. The other potential processes of selective assimilation by incorporation of Crd crystals or Sil-rich restites do not account for all these features of the Crd monzogranites.

Assessing the amount of assimilated material

The fraction of assimilated material in the Crd monzogranites can be estimated by two independent approaches. One is based on the amount of Crd, assuming that this mineral is the only recognizable phase of the assimilated material. The other approach is based on mass-balance calculations assuming that bulk assimilation is the dominant process. Both approaches are considered below.

Because Crd is the most easily recognizable phase from this complex process of peritectic reaction plus assimilation, it is expected that the amount of other unrecognized mineral phases and melt, which were produced together with Crd in the xenoliths, can be estimated if the fraction of Crd produced in the assimilated wall-rock xenoliths is known. Attempts to estimate the amount of assimilated material on the basis of the proportion of Crd measured in the hybrid rocks were made in the South Mountain batholith (Nova Scotia; Erdmann *et al.*, 2007). It is known from previous experimental studies that the fraction of Crd in metapelites strongly depends on pressure, temperature and bulk-rock composition (Stevens *et al.*, 1997). In our experimental results based on the composition of pelitic xenoliths from Gredos (20 wt % of added metapelite), the fraction of Crd is about 4% at conditions of 850°C and 400 MPa. Accordingly, the amount of assimilated material should be approximately five times the proportion of Crd in the granites, similar to the conclusion reached by Erdmann *et al.* (2007) in Nova Scotia. The Crd monzogranites, mapped in the Gredos area as part of this study, contain variable amounts of Crd ranging from 1 to 12 vol. %. The implication, therefore, is that the amount of assimilated material may range from 5 to 60 vol. %. In the case of more aluminous (more pelitic) compositions the fraction of Crd is increased and, thus, the amount of assimilated material will be lower compared with less aluminous compositions. Ugidos *et al.* (2008) reported an example of assimilation of compositionally exotic metasediments that produced more than 60 vol. % Crd. Obviously, such a process can produce a large amount of Crd in the magma from a small amount of assimilated material.

A two-component mixing test similar to that used in magma mixing calculations (Cantagrel *et al.*, 1984) has been applied in this study:

$$C_H = C_X a + C_M(1 - a) \quad (3)$$

$$a = (C_H - C_M)/(C_X - C_M) \quad (4)$$

where C_H is the composition of a hybrid, C_X the composition of the contaminant, C_M the composition of the

Table 5: Mixing tests for major elements based on the correlation of differences

XENOLITHS: Increase of pelitic component in the assimilant ↑	HYBRIDS: Distance from the assimilant in the diagram An-F-Or (Fig. 12) ←		
	Hybrid 1	Hybrid 2	Hybrid 3
Xenolith 1	a=0.14	a=0.24	a=0.39
	r^2=0.707	r^2=0.887	r^2=0.963
Xenolith 2	a=0.18	a=0.32	a=0.52
	r^2=0.644	r^2=0.841	r^2=0.929

a, mass fraction of the assimilated material; r^2, Pearson correlation coefficient.

intruding granodiorite, and a the fraction of the contaminant.

The estimation by mass balance is addressed by using the following end-member compositions. For the intruding magma (C_M) a Bt granodiorite with a composition falling at the intersection between the cotectic trend and the assimilation vector (Fig. 12) has been taken. For the contaminant (C_X), two xenoliths sampled in the mapped area close to the contact with the migmatitic hornfelses have been used. Several Crd monzogranites (C_H) were used to test the model for major elements. The two metasedimentary contaminants (xenoliths) have variable proportions of the pelitic (shale) component. The combination yields six mixing tests with differences in the mass fraction of the assimilated material (a) and in the value of the Pearson correlation coefficient (Table 5). By increasing the pelitic (shale) component, the fraction (a) of the contaminant decreases for a particular hybrid. Assuming that one volume fraction of Crd represent about five times the volume of digested material, 10 vol. % of Crd means that 50 vol. % of the present granitoid volume corresponds to assimilated material. These high values are restricted to local areas within a few metres of the contact with the migmatitic hornfelses. In these areas, the Crd monzogranites are rich in centimetre-sized xenoliths and Bt-rich schlieren. In areas more than 100 m from the contact, the amount of Crd may be less than 2 vol. %, which represents about 10 vol. % of assimilated material. Similar values were obtained by mass-balance calculation using the CaO content of the Crd monzogranites and the Bt granodiorites as the intrusive magmas (Ugidos & Recio, 1993). High proportions of assimilated crustal metasediments have also been estimated by mass-balance calculations based on Sr–Nd isotope compositions in other batholiths. These values include about 25% in the Caledonian Rogart granite (Fowler *et al.*, 2001) and 33% in the South Mountain batholith, Nova Scotia (Clarke *et al.*, 2004).

An estimation of the amount of contaminant based on trace element abundances cannot be made for several reasons. First, the intruding granodiorites are magmas that already have a crustal component inherited from their source. Their compositions can be close to those of metasediments (e.g. the REE patterns) and the effects of metapelite assimilation will therefore be difficult to identify. Second, and most important, late-stage magmatic differentiation processes (e.g. fluid migration) may modify the original trace element characteristics of the hybrid magma after the assimilation of pelitic country rocks. A rigorous assessment of assimilation on the basis of trace elements requires precise knowledge of the behaviour of those trace elements in fractionation processes, and this is far from well constrained at present. Our approach is therefore based on major element characteristics because these are fairly well constrained in terms of intensive variables that can be estimated by laboratory experiments. Also, major elements have a direct effect on the mineral assemblages that can be easily determined by direct observations of the rocks.

Regional importance of assimilation

The relative importance of the assimilation process on a regional scale can be estimated by the relative volume of the Crd-bearing granitoids with respect to the volume of the non-modified granodiorite. Excepting the Crd leucogranites that appear associated with pelitic migmatites, and some Crd monzogranites, containing mafic microgranular enclaves, that form shallow discordant plutons intrusive into the granodiorites (e.g. the Pedro Bernardo pluton in Gredos; Moreno-Ventas *et al.*, 1995) or even intrusive into low-grade metagreywackes (e.g. the Cabeza de Araya pluton; Vigneresse & Bouchez, 1997; García-Moreno *et al.*, 2006), the largest volumes of Crd-bearing granitoids are local facies of the intruding calc-alkaline granodiorites resulting from assimilation of country rocks. These

Crd-bearing granitoids form large masses in the Central System batholith. The results of this study in Gredos show that important mass fractions of about 0·2–0·5 of assimilated country rocks are present in the hybrid Crd monzogranites. Mapping of these hybrid facies in Gredos indicates that they occupy bands of several hundred metres thickness at the contacts with the pelitic country rocks. The geometry of the intruding bodies of granodiorite, consisting of subhorizontal sheets, favours magma–country rock interaction and enhances the generation of a large relative volume of modified granodiorite magma. Additionally, the significant abundance of pelitic metasediments in the Neoproterozoic and Early Paleozoic sequences that characterize the Variscan belt of Western Europe are important. The high probability that such materials form the country rocks of the calc-alkaline batholiths contributes significantly to the large volume of hybrid facies developed over large regions of the Variscan batholiths in Central Spain.

CONCLUDING REMARKS

The example of the Gredos Massif in the Central System batholith of the Spanish Variscan belt shows that assimilation of country rocks by silicate magmas is a potential mechanism to account for the particular geochemical and mineralogical features of Crd monzogranites. A process of bulk reactive assimilation is identified in this case. The apparently paradoxical observation of the presence of euhedral Crd crystals in strong disequilibrium within a non-anatectic monzogranite is compatible with the existence of local domains in which Crd was formed by the peritectic breakdown of Bt. Several independent lines of evidence point to bulk assimilation. Consequently, the fraction of Crd in the hybrid granitoids may be indicative of the total amount of digested material. At least locally, it is estimated that half of the mass of the Crd monzogranites has been gained by assimilation of country rocks. All these conclusions about bulk assimilation are valid for large areas of the studied batholith close to the contacts with pelitic metasediments. The Crd monzogranites change gradually to non-anatectic Bt granodiorites that were not affected by the assimilation process.

ACKNOWLEDGEMENTS

Careful reviews of the original manuscript by Barrie Clarke, James Beard and an anonymous reviewer are gratefully acknowledged. Richard Armstrong assisted with SHRIMP work at ANU, Canberra.

FUNDING

The paper is part of the PhD thesis of J.D.A., carried out at the Departments of Geology and Geodynamics and Palaeontology, University of Huelva with a Grant Fellowship from the Spanish Ministry of Science and Innovation (Grant no. AP2005-3489). The project was funded with Grants CGL2004-06808-CO4-01/BTE, CGL2004-06808-CO4-02/BTE and CGL2007-63237/BTE of the Spanish Ministry of Science and Innovation.

REFERENCES

Acosta-Vigil, A., London, D., Morgan, G. B., VI & Dewers, T. A. (2003). Solubility of excess alumina in hydrous granitic melts in equilibrium with peraluminous minerals at 700–800°C and 200 MPa, and applications of the aluminum saturation index. *Contributions to Mineralogy and Petrology* **146**, 100–119.

Barbey, P., Marignac, C., Montel, J. M., Macaudière, J., Gasquet, D. & Jabbori, J. (1999). Cordierite growth textures and the conditions of genesis and emplacement of crustal granitic magmas: The Velay granite complex (Massif Central, France). *Journal of Petrology* **40**, 1425–1441.

Bea, F., Montero, P. & Zinger, T. (2003). The nature, origin, and thermal influence of the granite source layer of Central Iberia. *Journal of Petrology* **111**, 579–595.

Bea, F., Montero, P., González Lodeiro, F., Talavera, C., Molina, J. F., Scarrow, J. H., Whitehouse, M. J. & Zinger, T. (2006). Zircon thermometry and U–Pb ion-microprobe dating of the gabbros and associated migmatites of the Variscan Toledo anatectic complex, Central Iberia. *Journal of the Geological Society, London* **163**, 847–855.

Bea, F., Montero, P., González-Lodeiro, F. & Talavera, C. (2007). Zircon inheritance reveals exceptionally fast crustal magma generation processes in Central Iberia during the Cambro-Ordovician. *Journal of Petrology* **48**, 2327–2339.

Beard, J. S., Ragland, P. C. & Crawford, M. L. (2005). Reactive bulk assimilation: A model for crust–mantle mixing in silicic magmas. *Geology* **33**, 681–684.

Burnham, C. W. (1979). The importance of volatile constituents. In: Yoder, H. S. J. (ed.) *The Evolution of the Igneous Rocks*. Princeton, NJ: Princeton University Press, pp. 439–482.

Cantagrel, J. M., Didier, J. & Gourgaud, A. (1984). Magma mixing: origin of intermediate rock and 'enclaves' from volcanism to plutonism. *Physics of the Earth and Planetary Interiors* **35**, 63–76.

Capdevila, R., Corretgé, L. G. & Floor, P. (1973). Les granitoides varisques de la Mesete Iberique. *Bulletin de la Société Géologique de France* **15**, 209–228.

Carroll, M. R. & Wyllie, P. J. (1990). The system tonalite–H_2O at 15 kbar and the genesis of calc-alkaline magma. *American Mineralogist* **75**, 345–357.

Castiñeiras, P., Villaseca, C., Barbero, L. & Martín Romera, C. (2008). SHRIMP U–Pb zircon dating of anatexis in high-grade migmatite complexes of central Spain: implications in the Hercynian evolution of Central Iberia. *International Journal of Earth Sciences* **97**, 35–50.

Castro, A. & Stephens, E. W. (1992). Amphibole-rich polycrystalline clots in calc alkaline granitic rocks and their enclaves. *Canadian Mineralogist* **30**, 1093–1112.

Castro, A., Patiño Douce, A., Corretgé, L. G., de la Rosa, J. D., el-Biad, M. & el-Hmidi, H. (1999). Origin of peraluminous granites and granodiorites, Iberian Massif, Spain: an experimental test of granite petrogenesis. *Contributions to Mineralogy and Petrology* **135**, 255–276.

Castro, A., Corretgé, L. G., El-Biad, M., El-Hmidi, H., Fernández, C. & Patiño Douce, A. (2000). Experimental constraints on

Hercynian anatexis in the Iberian Massif, Spain. *Journal of Petrology* **41**, 1471–1488.

Castro, A., Corretgé, L. G., De La Rosa, J., Enrique, P., Martínez, F. J., Pascual, E., Lago, M., Arranz, E., Galé, C., Fernández, C., Donaire, T. & López, S. (2002). Paleozoic magmatism. In: Gibbons, W. & Moreno, M. T. (eds) *The Geology of Spain*. London: Geological Society, pp. 117–153.

Castro, A., Gerya, T., Garcia-Casco, A., Fernandez, C., Diaz Alvarado, J., Moreno-Ventas, I. & Loew, I. (2010). Melting relations of MORB–sediment mélanges in underplated mantle wedge plumes. Implications for the origin of cordilleran-type batholiths. *Journal of Petrology* **51**, 1267–1295.

Chappell, B. W. & Stephens, W. E. (1988). Origin of infracrustal (I-type) granite magmas. *Transactions of the Royal Society of Edinburgh, Earth Sciences* **79**, 71–86.

Chappell, B. W. & White, A. J. R. (1974). Two contrasting granite types. *Pacific Geology* **8**, 173–174.

Clarke, D. B. (1995). Cordierite in felsic igneous rocks; a synthesis. *Mineralogical Magazine* **59**, 311–325.

Clarke, D. B. (2007). Assimilation of xenocrysts in granitic magmas: principles, processes, proxies and problems. *Canadian Mineralogist* **45**, 5–30.

Clarke, D. B., Macdonald, M. A. & Erdmann, S. (2004). Chemical variation in Al_2O_3–CaO–Na_2O–K_2O space: Controls on the peraluminosity of the South Mountain Batholith. *Canadian Journal of Earth Sciences* **41**, 785–798.

Collins, W. J. (1996). Lachlan Fold Belt granitoids: products of three component mixing. *Transactions of the Royal Society of Edinburgh, Earth Sciences* **87**, 171–181.

Cummings, G. L. & Richards, J. R. (1975). Ore lead isotope ratios in a continuously changing Earth. *Earth and Planetary Science Letters* **28**, 155–171.

Dallmeyer, R. D., Martínez Catalán, J. R., Arenas, R., Gil Ibarguchi, J. I., Gutiérrez Alonso, G., Farias, P., Aller, J. & Bastida, F. (1997). Diachronous Variscan tectonothermal activity in the NW Iberian Massif: evidence from $^{40}Ar/^{39}Ar$ dating of regional fabrics. *Tectonophysics* **277**, 307–337.

Días, G., Leterrier, J., Mendes, A., Simoes, P. P. & Bertrand, J. M. (1998). U–Pb zircon and monazite geochronology of post-collisional Hercynian granitoids from the Central Iberian Zone (Northern Portugal). *Lithos* **45**, 349–369.

Didier, J. & Lameyre, J. (1969). Les granites du Massif Central Français: étude comparée des leucogranites et granodiorites. *Contributions to Mineralogy and Petrology* **24**, 219–238.

Erdmann, S., London, D., Morgan, G. B., VI & Clarke, D. B. (2007). The contamination of granitic magma by metasedimentary country-rock material: An experimental study. *Canadian Mineralogist* **45**, 43–61.

Escuder Viruete, J., Arenas, R. & Martínez Catalán, J. R. (1994). Tectonothermal evolution associated with Variscan crustal extension in the Tormes Gneiss Dome (NW Salamanca, Iberian Massif, Spain). *Tectonophysics* **238**, 1–22.

Escuder Viruete, J., Hernáiz Huerta, P. P., Valverde Vaquero, P., Rodríguez Fernández, R. & Dunning, G. (1998). Variscan syncollisional extension in the Iberian Massif: structural, metamorphic and geochronological evidence from the Somosierra sector of the Sierra de Guadarrama (Central Iberian Zone, Spain). *Tectonophysics* **290**, 87–109.

Fernández, C., Becchio, R., Castro, A., Viramonte, J. M., Moreno-Ventas, I. & Corretgé, L. G. (2008). Massive generation of atypical ferrosilicic magmas along the Gondwana active margin: Implications for cold plumes and back-arc magma generation. *Gondwana Research* **14**, 451–473.

Fowler, M. B., Henney, P. J., Darbyshire, D. P. F. & Greenwood, P. B. (2001). Petrogenesis of high Ba–Sr granites: The Rogart pluton, Sutherland. *Journal of the Geological Society, London* **158**, 521–534.

Frost, B. R., Barnes, C. G., Collins, W. J., Arculus, R. J., Ellis, D. J. & Frost, C. D. (2001). A geochemical classification for granitic rocks. *Journal of Petrology* **42**, 2033–2048.

Garcia-Moreno, O., Castro, A., Corretgé, L. G. & El-Hmidi, H. (2006). Dissolution of tonalitic enclaves in ascending hydrous granitic magmas: An experimental study. *Lithos* **89**, 245–258.

Ghiorso, M. S. & Sack, R. O. (1995). Chemical mass transfer in magmatic processes. IV. A revised and internally consistent thermodynamic model for the interpolation and extrapolation of liquid–solid equilibria in magmatic systems at elevated temperatures and pressures. *Contributions to Mineralogy and Petrology* **119**, 197–212.

Grove, T. L., Baker, M. B. & Kinzler, R. J. (1984). Coupled CaAl–NaSi diffusion in plagioclase feldspar: Experiments and applications to cooling rate speedometry. *Geochimica et Cosmochimica Acta* **48**, 2113–2121.

Hoskin, P. W. O. & Black, L. P. (2000). Metamorphic zircon formation by solid-state recrystallization of protolith igneous zircon. *Journal of Metamorphic Geology* **18**, 423–439.

Johannes, W. & Holtz, F. (1996). *Petrogenesis and Experimental Petrology of Granitic Rocks*. Berlin: Springer.

Kretz, R. (1983). Symbols for rock-forming minerals. *American Mineralogist* **68**, 277–279.

Kuo, L. C. & Kirkpatrick, R. J. (1985). Dissolution of mafic minerals and its implications for the ascent velocities of peridotite-bearing basaltic magmas. *Journal of Geology* **93**, 691–700.

Le Breton, N. & Thompson, A. B. (1988). Fluid-absent (dehydration) melting of biotite in metapelites in the early stages of crustal anatexis. *Contributions to Mineralogy and Petrology* **99**, 226–237.

Lejeune, A. & Richet, P. (1995). Rheology of crystal-bearing silicate melts: an experimental study at high viscosities. *Journal of Geophysical Research* **100**, 4215–4229.

Maaløe, S. & Wyllie, P. J. (1975). Water content of a granite magma deduced from the sequence of crystallization determined experimentally with water-undersaturated conditions. *Contributions to Mineralogy and Petrology* **52**, 175–191.

Martínez Catalán, J. R., Fernández Suárez, J., Jenner, G. A., Belousova, E. & Díez Montes, A. (2004). Provenance constraints from detrital zircon U–Pb ages in the northwestern Iberian Massif: implications for Paleozoic plate configuration and Variscan evolution. *Journal of the Geological Society, London* **161**, 461–473.

McLaren, A. C., Fitz Gerald, J. D. & Williams, I. S. (1994). The microstructure of zircon and its influence on the age determination from Pb/U isotopic ratios measured by ion microprobe. *Geochimica et Cosmochimica Acta* **58**, 993–1005.

Montero, P., Bea, F., Zinger, T. F., Scarrow, J. H., Molina, J. F. & Whitehouse, M. (2004). 55 million years of continuous antexis in Central Iberia: single-zircon dating of the Peña Negra Complex. *Journal of the Geological Society, London* **161**, 255–263.

Montero, P., Bea, F., González-Lodeiro, F., Talavera, C. & Whitehouse, M. J. (2007). Zircon ages of the metavolcanic rocks and metagranites of the Ollo de Sapo Domain in central Spain: implications for the Neoproterozoic to Early Palaeozoic evolution of Iberia. *Geological Magazine* **144**, 963–976.

Moreno-Ventas, I. (1991). Petrología de Granitoides y Rocas Básicas Asociadas de la Sierra de Gredos, Sistema Central Español, Ph.D. Thesis, University of Seville, 324 pp.

Moreno-Ventas, I., Rogers, G. & Castro, A. (1995). The role of hybridization in the genesis of Hercynian granitoids in the Gredos

massif, Spain: inferences from Sr–Nd isotopes. *Contributions to Mineralogy and Petrology* **120**, 137–149.

Nakamura, N. (1974). Determination of REE, Ba, Fe, Mg, Na and K in carbonaceous and ordinary chondrites. *Geochimica et Cosmochimica Acta* **38**, 757–773.

Naney, M. T. (1983). Phase equilibria of rock forming ferromagnesian silicates in granitic systems. *American Journal of Science* **283**, 993–1033.

Paterson, S. R. & Janousek, V. (2008). Growth of complex sheeted zones during recycling of older magmatic units into younger: Sawmill Canyon area, Tuolumne batholith, Sierra Nevada, California. *Journal of Volcanology and Geothermal Research* **177**, 457–484.

Patiño Douce, A. E. (1992). Calculated relationships between activity of alumina and phase assemblages of silica-saturated igneous rocks. Petrogenetic implications of magmatic cordierite, garnet and aluminosilicate. *Journal of Volcanology and Geothermal Research* **52**, 43–63.

Patiño Douce, A. E. (1999). What do experiments tell us about the relative contributions of crust and mantle to the origin of granitic magmas? In: Castro, A., Fernández, C. & Vigneresse, J. L. (eds) *Understanding Granites Integrating New and Classical Techniques. Geological Society, London, Special Publications* **168**, 55–75.

Patiño Douce, A. E. & Beard, J. S. (1996). Effects of P, f(O2) and Mg/Fe ratio on dehydration-melting of model metagreywackes. *Journal of Petrology* **37**, 999–1024.

Patiño Douce, A. E. & Johnston, A. D. (1991). Phase equilibria and melt productivity in the pelitic system: implications for the origin of peraluminous granitoids and aluminous granulites. *Contributions to Mineralogy and Petrology* **107**, 202–218.

Pereira, M. D. & Bea, F. (1994). Cordierite-producing reactions in the Peña Negra complex, Avila batholith, Central Spain: the key role of cordierite in low-pressure anatexis. *Canadian Mineralogist* **32**, 763–780.

Philpotts, J. A. & Schnetzler, C. C. (1970). Phenocryst–matrix partition coefficients for K, Rb, Sr and Ba with applications to anorthosite and basalt genesis. *Geochimica et Cosmochimica Acta* **34**, 307–322.

Pichavant, M., Costa, F., Burgisser, A., Scaillet, B., Martel, C. & Poussineau, S. (2007). Equilibration scales in silicic to intermediate magmas implications for experimental studies. *Journal of Petrology* **48**, 1955–1972.

Pin, C. & Duthou, J. L. (1990). Sources of Hercynian granitoids from the French Massif Central: Inferences from Nd isotopes and consequences for crustal evolution. *Chemical Geology* **83**, 281–296.

Rapela, C. W., Baldo, E. G., Pankhurst, R. J. & Saavedra, J. (2002). Cordieritite and leucogranite formation during emplacement of highly peraluminous magma: the El Pilón granite complex (Sierras Pampeanas, Argentina). *Journal of Petrology* **43**, 1003–1028.

Saito, S., Arima, M. & Nakajima, T. (2007). Hybridization of a shallow 'I-type' granitoid pluton and its host migmatite by magma-chamber wall collapse: The Tokuwa pluton, Central Japan. *Journal of Petrology* **48**, 79–111.

Sisson, T. W., Ratajeski, K., Hankins, W. B. & Glazner, A. F. (2005). Voluminous granitic magmas from common basaltic sources. *Contributions to Mineralogy and Petrology* **148**, 635–661.

Skjerlie, K. P. & Patiño Douce, A. E. (2002). The fluid-absent partial melting of a zoisite-bearing quartz eclogite from 1·0 to 3·2 GPa; implications for melting in thickened continental crust and for subduction zone processes. *Journal of Petrology* **43**, 291–314.

Steiger, R. H. & Jäger, E. (1977). Subcommission on geochronology: convention on the use of decay constants in geo- and cosmochronology. *Earth and Planetary Science Letters* **36**, 359–362.

Stephens, W. E. & Halliday, A. N. (1984). Geochemical contrasts between late Caledonian granitoid plutons of northern, central and southern Scotland. *Transactions of the Royal Society of Edinburgh: Earth Sciences* **75**, 259–273.

Stevens, G., Clemens, J. D. & Droop, G. T. R. (1997). Melt production during granulite facies anatexis: Experimental data from 'primitive' metasedimentary protoliths. *Contributions to Mineralogy and Petrology* **128**, 352–370.

Thompson, A. B. (1982). Dehydration melting of pelitic rocks and the generation of H_2O-undersaturated granitic liquids. *American Journal of Science* **282**, 1567–1595.

Thompson, A. B. (1996). Fertility of crustal rocks during anatexis. *Transactions of the Royal Society of Edinburgh: Earth Sciences* **87**, 1–10.

Tsuchiyama, A. (1985). Dissolution kinetics of plagioclase in the melt of the system diopside–albite–anorthite, and origin of dusty plagioclase in andesites. *Contributions to Mineralogy and Petrology* **89**, 1–16.

Tuttle, O. F. & Bowen, N. L. (1958). *Origin of granites in the light of experimental studies in the system $NaAlSi_3O_8$–$KAlSi_3O_8$–SiO_2–H_2O. Geological Society of America, Memoirs* **74.**

Ugidos, J. M. & Recio, C. (1993). Origin of cordierite-bearing granites by assimilation in the Central Iberian Massif (CIM), Spain. *Chemical Geology* **103**, 27–43.

Ugidos, J. M., Stephens, W. E., Carnicero, A. & Ellam, R. M. (2008). A reactive assimilation model for regional-scale cordierite-bearing granitoids: geochemical evidence from the Late Variscan granites of the Central Iberian Zone, Spain. *Earth and Environmental Science Transactions of the Royal Society of Edinburgh* **99**, 225–250.

Valverde-Vaquero, P. & Dunning, G. R. (2000). New U–Pb ages for Early Ordovician magmatism in central Spain. *Journal of the Geological Society, London* **157**, 15–26.

Van der Molen, I. & Paterson, M. S. (1979). Experimental deformation of partially melted granite. *Contributions to Mineralogy and Petrology* **70**, 299–318.

Vielzeuf, D. & Holloway, J. R. (1988). Experimental determination of the fluid-absent melting relations in the pelitic system. *Contributions to Mineralogy and Petrology* **98**, 257–276.

Vigneresse, J. L. & Bouchez, J. L. (1997). Successive granitic magma batches during pluton emplacement: The case of Cabeza de Araya (Spain). *Journal of Petrology* **38**, 1767–1776.

Williams, I. S. & Claesson, S. (1987). Isotopic evidence for the Precambrian provenance and Caledonian metamorphism of high grade paragneisses from the Seve Nappes, Scandinavian Caledonides, II Ion microprobe zircon U–Th–Pb. *Contributions to Mineralogy and Petrology* **97**, 205–217.

Wingate, M. T. D., Campbell, I. H., Compston, W. & Gibson, G. M. (1998). Ion microprobe U–Pb ages for Neoproterozoic basaltic magmatism in south-central Australia and implications for the breakup of Rodinia. *Precambrian Research* **87**, 135–159.

Winkler, H. G. F. & Lindemann, W. (1972). The system Qz–Or–An–H2O in the granite system Qz–Or–Ab–An–H2O. Applications to granite magma formation. *Neues Jahrbuch der Mineralogie, Monatschefte* 49–61.

Zeck, H. P. & Whitehouse, M. J. (2002). Repeated age resetting in zircons from Hercynian–Alpine polymetamorphic schists (Betic–Rif tectonic belt, S. Spain); a U–Th–Pb ion microprobe study. *Chemical Geology* **182**, 275–292.

Zeck, H. P., Wingate, M. T. D., Pooley, G. D. & Ugidos, J. M. (2004). A sequence of Pan-African and Hercynian events recorded in zircons from an orthogneiss from the Hercynian belt of Western Central Iberia—an ion microprobe U–Pb study. *Journal of Petrology* **45**, 1613–1629.